CrossMark

ORIGINAL ARTICLE

Biosorption of As(III) and As(V) on the surface of TW/MnFe$_2$O$_4$ composite from wastewater: kinetics, mechanistic and thermodynamics

M. S. Podder[1] · C. B. Majumder[1]

Abstract In the present study, TW/MnFe$_2$O$_4$ composite (MTW) was synthesized and estimated as an effective biosorbent for removing As (III) and As(V) from wastewater. Physicochemical analysis of composite was performed through SEM–EDX. 86.615 and 83.478% removal efficiency were obtained by composite dosage of 2 g/L at contact time 120 min at temperature 30 °C and pH 7.0 and 4.0 for As(III) and As(V), respectively. Kinetic results study showed that Brouers–Weron–Sotolongo and Ritchie second-order for As(III) and Brouers–Weron–Sotolongo model for As(V) were capable to describe an accurate explanation of adsorption kinetic. Applicability of mechanistic models in the current study exposed that the rate-controlling step in the biosorption of both As(III) and As(V) on the surface of composite was film diffusion rather than intraparticle diffusion. The estimated thermodynamic parameters ΔG^0, ΔH^0 and ΔS^0 revealed that the biosorption of both As(III) and As(V) on the composite was feasible, spontaneous and exothermic.

Keywords Arsenic · Biosorption · Kinetic · Mechanistic · Thermodynamic · Modelling

✉ M. S. Podder
mou.chem11@gmail.com

C. B. Majumder
cbmajumder@gmail.com

[1] Department of Chemical Engineering, Indian Institute of Technology, Roorkee, Roorkee 247667, India

Nomenclature

a_E	Elovich coefficient representing the initial adsorption rate (mg/g min)
b_E	Elovich coefficient representing desorption constant (g/mg)
A	The frequency factor
B_{bt}	A mathematical function of F ($F = q_t/q_e$)
C_0	Initial concentration of arsenic in the solution (mg/L)
C_e	Equilibrium concentration of arsenic in the solution (mg/L)
C_s	The concentration of arsenic on the adsorbent and in the solution (mg/L)
C_{int}	The intercept of the intraparticle diffusion plot (mg/g)
d	The thickness of the water film adhered to the adsorbent (cm)
D_1	Film diffusion constant (cm^2/s)
D_2	Pore diffusion constant (cm^2/s)
D_e	Diffusivity (m^2/s)
D_f	Film diffusion coefficient (cm^2/s)
D_p	Pore diffusion coefficient (cm^2/s)
E_a	The activation energy of adsorption characterizing the distribution (kJ/mol)
F	The adsorption progress ($F = q_t/q_e$)
f_2	The involvement of pseudo second-order model
f_{eq}	The Langmuir batch equilibrium factor
h	The initial adsorption rate (mg/g min)
$k'_{1,0}$	The fractal-like mixed 1, 2 order rate coefficient (1/min)$^\alpha$
k'_{2R}	The modified second-order rate coefficient (1/min)
k''_{2R}	The Ritchie second-order rate coefficient (1/min)
k_{AV}	The Avrami kinetic rate coefficient (1/min)
$k_{a,obs}$	The acquired rate coefficients of adsorption

$k_{d,obs}$	The acquired rate coefficients of desorption	t	Contact time (min)
k_b	The Bangham model constant (mL/g L)	$t_{(1/2)}$	The time necessary for the adsorbate concentration to fall to half the initial concentration (s)
k_d	The adsorption equilibrium constant (L/g)		
k_{DW}	The Dumwald–Wagner rate constant (1/min)		
k_{EXP}	The exponential rate coefficient (mg/g min)	t^α	A fractal time
k_{int}	The intraparticle diffusion rate coefficient (mg/ g min$^{0.5}$)	T	The absolute temperature (K)
		u_{eq}	Relative equilibrium uptake
k_M	The film diffusion rate constant (1/min)	v	Adjustment parameter
k_{MOE}	The mixed 1, 2 order rate coefficient (1/min)	V	The volume of the solution (mL)
$k_{nBWS,\alpha}$	The reaction constant (1/min)		

Greek symbols

k_{PF}	The fractional power model rate constant (mg/ g min)	α	The fractal time exponent
		α_b	Bangham model constant
k_{PFO}	The pseudo first-order rate coefficient (1/min)	θ	The adsorbent surface coverage at pre-adsorbed stage, ($\theta = q_t/q_e$) dimensionless
k_{PSO}	The pseudo second-order rate coefficient (g/ mg min)		
		θ_0	The adsorbent surface coverage at time t, ($\theta_0 = q_0/q_e$) dimensionless
k'_{EXP}	Division of k_{EXP} by q_e (1/min)		
k''_{EXP}	The fractal-like exponential rate coefficient (1/min)	θ_e	The relative surface coverage at equilibrium
		$\tau_{1/2}$	Half-reaction time (min)
k'_{PFO}	The fractal-like pseudo first-order kinetic rate coefficient (1/min)	$\tau_{nBWS,\alpha}$	The time required for adsorbing half the maximum amount
k'_{FPFO}	The fractal-like pseudo first-order kinetic rate coefficient (1/min)$^\alpha$	ΔG^0	Gibbs free energy change (kJ/mol)
		ΔH^0	Enthalpy change (kJ/mol)
k'_{FPSO}	The fractal-like pseudo second-order kinetic rate coefficient (g/mg min)$^\alpha$	ΔS^0	Entropy change (J/mol K)
k'_{PSO}	Multiplication of q_e and k_{PSO} (1/min)		
k''_{FPSO}	Multiplication of q_e and k'_{FPSO} (1/min)		
M	The mass of the biosorbent (dry) (g)		
m	The weight of the adsorbent per liter of solution (g/L)		
m_b	An integer that describes infinite series solution		
n	The number of observations in the experimental study		
n_{AV}	Constant corresponding to the mechanism of adsorption		
n_{BWS}	A fractional reaction order		
n_R	Number of surface sites		
p	The number of parameters to be estimated		
q_e	The amount of adsorbate adsorbed on the adsorbent surface at equilibrium (mg/g)		
q_m	The adsorption capacity		
q_t	The amount of adsorbate adsorbed on the adsorbent surface at time t (mg/g)		
$q_{t,exp}$	The biosorption capacity observed from the batch experiment after time t (mg/g)		
$q_{t,model}$	The calculation from the kinetic model corresponding to C_t		
r	Mean radius of adsorbent particle (assumed spherical) (cm)		
r_a	The rate of adsorption		
r_d	The rate of desorption		
R	The universal gas constant (8.314 J/mol K)		
R_e	% removal		

Introduction

Contamination of natural arsenic (As) in water supplies is a main environmental and health problem on a worldwide scale. Concentrations of arsenic in groundwater and surface water in many regions of the world are increasing in current years (Ferguson and Gavis 1972; Smedley and Kinniburgh 2002; Mohan and Pittman 2007; Ravenscroft et al. 2009). The natural processes responsible for the environmental distribution of arsenic are weathering reactions, volcanic emissions and biological activities. The anthropogenic activities responsible for the arsenic contamination are smelting, glass and ceramic manufacturing industries, insecticides and petroleum refineries (Kundu and Gupta 2006; Mondal et al. 2006; Mohan and Pittman 2007).

Copper smelting creates a huge volume of wastewater containing large amounts of inorganic compounds such as heavy metals like lead, copper, zinc, iron, cadmium and bismuth and highly carcinogenic metalloid like arsenic species. It poses a serious threat towards man and the flora and fauna of our ecosystem contaminating the natural water tables (ground water and surface water) in the vicinity. In copper smelting, wastewater concentration of arsenic is as high as 1979 mg/L (Basha et al. 2008). With the aim of maintaining a good quality of fresh water resources, this wastewater must be treated so that the water can be reverted to the ecosystems.

Arsenic occurs as a major component in more than 200 minerals, such as elemental arsenic, orpiment, galena, arsenopyrites, marcasite and realgar. Two dominating species of inorganic forms of arsenic which exist in natural water are arsenite (As(III)) and arsenate (As(V)). Arsenite (As(III)) is usually more mobile and toxic than arsenate (As(V)) as the predominant As(III) compound is neutral in charge (Korte and Fernando 1991; Neff 1997). Contamination of arsenic in drinking water is gradually increasing. It enters into the blood from water, gets concentrated with time and causes cancer of liver, prostate, kidney, skin, lungs and bladder. It is one of the probable risks to instigate hyperkeratosis and change in skin pigmentation (Meng et al. 2000, 2002; Mondal et al. 2006). Long-term exposure of arsenic terminates the function of nervous system and cardiovascular, which may finally lead to death.

Owing to the severe effects of arsenic on people's health, the maximum contaminant level (MCL) of arsenic in drinking water has been revised from 50 to 10 µg/L by the World Health Organization (WHO 1993) and the European Commission in 2003 (European commission Directive, 98/83/EC 1998). However, many countries including Bangladesh and China have kept the drinking water standard as 50 µg/L as the prior WHO guideline. United States Environmental Protection Agency (EPA report-816-D-02-005 1998) has also recommended the MCL of arsenic in drinking water as 10 µg/L. The MCL of arsenic in drinking water has been set as 7 µg/L by National Health and Medical Research Committee (NHMRC), Australia (NHMRC 1996). Therefore, processes to scavenge arsenic competently from drinking water and wastewater with concentrations >0.01 mg/L are urgently required.

Several physicochemical techniques are applied for removing arsenic from both water and wastewater. The conventional methods used for the removal of arsenic are membrane techniques, oxidation/precipitation, ion exchange, coagulation and flocculation and adsorption (Dambies 2004; Garelick et al. 2005; Mondal et al. 2006; Wang and Mulligan 2006; Choong et al. 2007; Mohan and Pittman 2007). However, these methods suffer from several disadvantages such as inadequate removal of metal ions, high capital as well as high operational cost, limited tolerance to pH change, and energy requirements. They are inappropriate for small-scale industries, and disposal of the remaining toxic metal containing sludge which needs to be further treated is also a problem (Sharma and Sohn 2009; Chiban et al. 2011). Adsorption processes are operative practices and they have long been applied in industries for abating inorganic and organic pollution for low budget, easy treatment, minimal sludge production and its regeneration ability. (Ranjan et al.

2009). The response of biotechnological prospective has praised researches for gaining alternative processes of heavy metal removal techniques which can revenue both the environment and the economy. These have led to an up-and-coming technology named biosorption.

Biosorption is demarcated as a procedure using an appropriate dead biomass for adsorbing metal ions from aqueous solutions (Jeffers et al. 1991). The high affinities between the adsorbate, in this case metal ions and biosorbents, attract and bind them in different mechanisms (Ramachandra et al. 2005). These mechanisms include complexation, coordination, physiochemical mechanisms, electrostatic interaction, ion exchange combinations, micro-precipitation, adsorption and chelation (Vijayaraghavan and Yun 2008; Wang and Chen 2006).

The attentive selection of the most suitable replacements should be on the basis of a cost-benefit analysis done for each one of the potential removal techniques. At this stage, development in the awareness of biosorption has gained robust consistency during recent years due to its eco-friendly nature, very profitable, exceptional performance, vigorous process and less costly domestic practice for remediating even tremendously metal-contaminated water (Volesky 2001). Most of biosorbents are simply available, inexpensive and there is no requirement of extra nutrients. Furthermore, biosorption produces no secondary chemical sludge; besides, biosorbents can be readily regenerated which aids in recovery of metal ion (Park et al. 2008; Chubar et al. 2004). But still, there lies a big challenge to develop biosorbents to remove arsenic with high removal efficiency, inexpensive and well-explained biosorption mechanism.

Surface modification of biosorbents is appealing as a current research field for the advance of low-cost arsenic removal technique. Recently, some biosorbents like iron-coated rice husk (Pehlivan et al. 2013), iron-modified bamboo charcoal (Liu et al. 2012), magnetic wheat straw (Tian et al. 2011), magnetic biochar (Zhang et al. 2013), magnetite-doped activated carbon fiber (Zhang et al. 2010a) and iron–chitosan composites (Gupta et al. 2009) were described for efficient biosorption. Due date, Zhang et al. (2010b) described that bimetal oxide magnetic nanomaterials ($MnFe_2O_4$ and $CoFe_2O_4$) were synthesized and characterized and used for removing of As(III) and As(V). Parsons et al. (2009) stated the ability of the Fe_3O_4, Mn_3O_4, and $MnFe_2O_4$ nanophases for removing As(III) and As(V) from aqueous solutions.

Tea waste is a household waste obtainable in huge quantity in India as well as all over the world. It is an oxygen-demanding pollutant. Besides, it takes a long time for biodegradation. Conversely, while the tea waste used as biosorbent becomes saturated, it is just incinerated. The waste tea ash acquired by incineration is not a pollutant;

rather, it could be utilized as a biosorbent. So, tea waste is a cost-effective biosorbent (Uddin et al. 2009). In this current investigation, the household tea waste was used as template, and $MnFe_2O_4$ particles were grown. A composite of tea waste and $MnFe_2O_4$ particles was prepared, and then, its probable application in arsenic biosorption was explored. Insoluble cell walls of tea leaf are mainly made up of hemicelluloses and cellulose, structural proteins, and several hydroxyl-rich compounds like condensed tannins and lignin (Tee and Khan 1988; Zakaria et al. 2007). The hydroxyl groups can offer chemical reaction sites and adsorb iron and manganese ions to grow $MnFe_2O_4$ particles.

$MnFe_2O_4$, a familiar soft material, has outstanding chemical stability and frequently controls the concentration of free metal and organic matter in water or soil through adsorption reactions (Backes et al. 1995; Muroi et al. 2001). In the present work, a composite of tea waste/$MnFe_2O_4$ (TW/$MnFe_2O_4$) was synthesized to hybridize high adsorption capacity of $MnFe_2O_4$ with biosorptivity of tea waste. So, TW/$MnFe_2O_4$ composite having the advantages of preferred biosorption capacity, could be used as an economical and encouraging biosorbent to remove a wide range of arsenic. The use of chemically modified adsorbent/biosorbent for adsorption/biosorption of arsenic ions from water is an extremely effective process, due to which it is becoming widespread day by day. Podder and Majumder (2016) examined the potential of SD/$MnFe_2O_4$ composite to biosorb both As(III) and As(V) in batch experimentations targeting the treatment of wastewater with high concentrations. Podder and Majumder (2015) also reported the use of GAC/$MnFe_2O_4$ composite for the removal of arsenic from wastewater. But compared to those, adsorbent/biosorbent TW/$MnFe_2O_4$ composite is cost-effective because tea waste is a household waste and is readily available and cheap. Furthermore, to our best knowledge, nothing is known about the efficiency of TW/$MnFe_2O_4$ composite in arsenic removal from wastewater.

The purposes of the present study, divided into six parts, were (1) to characterize the prepared TW/$MnFe_2O_4$ composite with BET surface area and SEM–EDX, (2) to examine the influence of contact time in addition to temperature for removing As(III) and As(V) from synthetically prepared copper smelting wastewater, (3) to evaluate the kinetics and mechanism of present biosorption process, (4) to examine the biosorption thermodynamics to identify the biosorption mechanism, (5) to investigate the influence of initial arsenic concentration on biosorption kinetics and (6) to verify the influence of temperature on biosorption kinetics.

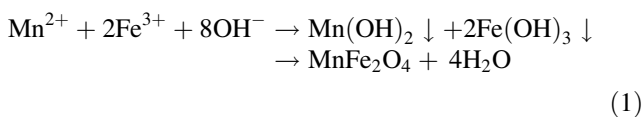## Materials and methods

Materials

Tea waste was collected from the tea stall located in the campus of Indian institute of Technology, Roorkee, India. The stock solutions of As(III) and As(V) were prepared by dissolving sodium arsenite ($NaAsO_2$) and sodium arsenate (Na_2HAsO_4, $7H_2O$), purchased from HiMedia Laboratories Pvt. Ltd., Mumbai, India, in 1 L of double-distilled water, respectively. All other required chemicals utilized in the experiments, were of analytical reagent grade and were purchased from HiMedia Laboratories Pvt. Ltd., Mumbai, India.

Preparation of TW/MnFe₂O₄ composite (MTW)

Tea waste (TW) with a particle size of 1.18 mm diameter was washed for cleaning the adhering dirt, rinsed methodically with double-distilled water and, last of all, heated in an air oven at 105 °C for 4 h. 25 g of dried TW was added into 500-mL conical flask containing 250 mL of 0.5 M HCl solution and, next, was agitated for 4 h at 120 rpm at 25 °C. Thereafter, the mixture was left overnight. Then, the mixture was filtered for separating TW which was continually washed with double-distilled water for providing neutral pH. Then, the biosorbents were dried at 110 °C for 3 h for removing moisture, cooled to room temperature and kept in plastic bags for further usage.

TW/$MnFe_2O_4$ composites were prepared by chemical coprecipitation method with few changes (Shao et al. 2012). In this procedure, 11.52 g of acid-treated TW was mixed into 200 mL solution containing dissolved ferric (III) chloride ($FeCl_3$) (0.05 mol i.e. 8.11 g) and manganese (II) chloride ($MnCl_2$) (0.025 mol i.e. 3.146 g) at room temperature. The amount of acid-treated TW was fixed for procuring TW/$MnFe_2O_4$ mass ratios of 2:1. The solution temperature was increased to 60 °C under energetic magnetic stirring, and after that, 5 mol/L of NaOH solution was added drop by drop to the above mixture till the pH of the solution reached 11. Then next, 1 h shaking was continued. Then, the suspension was heated in a water bath at 100 °C for 4 h. After cooling, the prepared composite was repeatedly washed with double-distilled water to eliminate the contaminations (e.g. Na^+, Cl^-) accompanied with the processes. Later, as-prepared composite was collected from the washed solution by filtering the mixture and, then, was dried at 110 °C in an air oven. Fig. S1 of supplementary material represents the schematic diagram for the preparation of composite biosorbent. The reaction ionic equation (Bianfang et al. 2007) is as follows:

$$Mn^{2+} + 2Fe^{3+} + 8OH^- \rightarrow Mn(OH)_2 \downarrow + 2Fe(OH)_3 \downarrow$$
$$\rightarrow MnFe_2O_4 + 4H_2O$$

$$(1)$$

$$MnFe_2O_4 + TW \rightarrow TW - MnFe_2O_4 \qquad (2)$$

Batch experimental studies and analytical methods

All biosorption experiments were carried out by agitating an optimum biosorbent dose of 2 g/L of the TW/MnFe$_2$O$_4$ composite with 100 mL synthetically prepared copper smelting wastewater of As(III) or As(V) of necessary concentration, at an optimum initial pH value around 7.0 and 4.0, respectively, and at a desired temperature, in an incubator cum orbital shaker (REMI Laboratory instruments) at 120 rpm. 1.0 N NaOH and 1.0 N HCl solutions were used for regulating the initial pH of the solution utilizing a digital pH meter (HACH$^®$ India).

To inspect the influence of temperature on biosorption, batch experiments were done by contacting an optimum biosorbent dose (2 g/L) of the TW/MnFe$_2$O$_4$ composite with As(III) or As(V) solution of a fixed concentration (50 mg/L) at an optimum contact time of 120 min at a range of temperatures (20, 25, 30, 40, 45 and 50 °C).

To observe the biosorption kinetics, batch experiments were performed by contacting an optimum biosorbent dose (2 g/L) of the TW/MnFe$_2$O$_4$ composite with As(III) or As(V) solution of a fixed concentration (50 mg/L) at a constant temperature (30 °C).

To review the effect of initial concentration on the kinetics of biosorption of both As(III) and As(V) by TW/MnFe$_2$O$_4$ composite, all biosorption experiments were done by agitating 2 g/L of the TW/MnFe$_2$O$_4$ composite with 100 mL of As(III) or As(V) of selected concentration (50–2000 mg/L) at a constant temperature (30 °C). Experiments were done for six initial concentrations (50, 100, 500, 1000, 1500 and 2000 mg/L) by agitating the flasks.

To investigate the influence of temperature on the kinetics of biosorption of both As(III) and As(V) by TW/MnFe$_2$O$_4$ composite, 2 g/L TW/MnFe$_2$O$_4$ composite was added to each round-bottom flask containing 50 mg/L solution of As(III) or As(V). Experiments were conducted at three temperatures (30, 40 and 50 °C) by shaking the flasks.

The samples were collected from the flasks through filtration by Whatman filter paper (Cat No 1001 125) (Remi Instruments Ltd., Mumbai, India) after fixed contact time for thermodynamic studies as well as at predetermined time intervals for kinetic studies, and a part of filtrate was diluted with HNO$_3$ solution (10%, v/v). The filtrate was analysed to determine arsenic concentration utilizing Thermo Fisher Scientific iCE 3000 series AA graphite furnace atomic absorption (GFAA) spectrometer (detection limit 20 μg/L).

Characterization

Scanning electron microscope (SEM; LEO Electron Microscopy, England) was used to characterize the surface morphology of TW/MnFe$_2$O$_4$ composite. The solid samples were spread on adhesive carbon tape supported on metallic disks. Before and after arsenic biosorption, the elemental compositions of TW/MnFe$_2$O$_4$ composite were determined by arbitrarily choosing areas on the surfaces of solid and then analysed by energy-dispersive X-ray (EDX) along with SEM.

Theoretical background

With the goal of assessing biosorption capacity by mass balance, detailed as the amount of adsorbate molecules adsorbed per unit mass of biosorbent at time t (mg/g), was calculated as follows:

$$q_t = (C_0 - C_t)\frac{V}{M}. \qquad (3)$$

The amount of adsorbate molecules adsorbed in terms of percentage was calculated as follows:

$$R_e\,(\%) = \frac{(C_0 - C_t)}{C_0} \times 100. \qquad (4)$$

Determining adsorption kinetic parameters by non-linear regression

The kinetic parameter sets are computed by non-linear regression because of the inherent bias caused after linearization. This offers a mathematically laborious method to evaluate kinetic parameters utilizing the original kinetic equation (Khan et al. 1996; Ncibi 2008; Hadi et al. 2012). Commonly, Gauss–Newton methods or Levenberg–Marquardt-based algorithms (Edgar and Himmelblau 1989; Hanna and Sandall 1995) are utilized. The biosorption kinetic data of arsenic on TW/MnFe$_2$O$_4$ composite were analysed by non-linear curve fitting analysis using professional graphics software package OriginPro (8.5.1 version) for fitting the kinetic models.

The optimization method requires the selection of a goodness-of-fit measure (GoFM) with the purpose of valuing the fitting of the kinetics to the experimental data. In the present research, six GoFM (residual sum of squares (SSE), reduced Chi-squared test (reduced χ^2), coefficient of determination (R^2), adjusted R-square ($\overline{R^2}$), R value (R) and root-MSE value were employed for evaluating kinetic parameters utilizing the OriginPro software by considering

95% confidence interval (the details are provided with the supplementary material).

The adjusted coefficient of determination ($\overline{R^2}$), which generally takes into account the number of variables and sample size in the model, is deliberated superior to the coefficient of determination (R^2), since it revises the overestimation by R^2 (Warrens 2008). While dealing with small samples, specifically, it is more exact than R^2.

Adsorption kinetic modelling

Biosorption kinetics reveals the rate of adsorbates bonding on the surface of the biological materials. Kinetics studies deliver the vital information about the probable mechanism of biosorption that includes the diffusion (bulk, external, and intraparticle) and chemical reactions. In general, it is supposed that adsorbate transport happens in the few following steps. The first step includes the transport of adsorbate in the bulk of the solution; second step comprises the external diffusion or film diffusion (the substrates diffuse from the bulk solution to the external surface of the biosorbent); the third step was because of the transport of the adsorbate across the boundary layer; the fourth step involves the transfer of compounds in the pores to the internal parts of the biosorbent; and finally, uptake of molecules by the active sites which is so-called internal diffusion or intraparticle diffusion, and the fifth step comprises biosorption and desorption between the adsorbate and active sites, i.e., mass action (Plazinski et al. 2009; Qiu et al. 2009; Michalak et al. 2013). In many experimental biosorption systems, the influence of transport in the solution is rejected by fast mechanical mixing, so it is not supposed to be involved in governing of the overall sorption rate and can be overlooked, as a rule (Plazinski et al. 2009). In the past decades, several mathematical models have been proposed to describe adsorption data, which can usually be categorized as adsorption reaction models and adsorption diffusion models. Both models are used to describe the kinetic process of biosorption; but, they are quite different in nature. Adsorption diffusion models are always constructed on the basis of above five consecutive steps. However, adsorption reaction models originating from chemical reaction kinetics are on the basis of the whole process of adsorption without considering these steps mentioned above. Both adsorption reaction models and adsorption diffusion models are now widely employed for fitting kinetic data (Qiu et al. 2009).

With the purpose of inspecting dynamic biosorption behaviour of As(III) and As(V) on the surface of TW/MnFe$_2$O$_4$ composite, i.e., controlling the current biosorption process mechanisms and the possible rate-controlling

steps, e.g., mass transport and/or chemical biosorption processes, kinetic models have been used to fit the experimental data. Fourteen kinetic models were used in the present study assuming that concentrations on the biosorbent surface are equal to the measured concentrations.

There are many models for kinetics of biosorption at the interface of solid/solution. Fractional power model (FP), pseudo first-order (PFO) and pseudo second-order (PSO) are common empirical models; however, their major drawback is that they may simply define the kinetics of adsorption at some restrictive situations (Haerifar and Azizian 2013). Elovich is a two-parametric semi-empirical model, and fractional power (FP), Ritchie second-order, and exponential (EXP) kinetic models are two-parametric empirical models to analyze kinetic data at near to equilibrium. As well, other empirical models, for instance, Avrami, modified pseudo second-order (MPSO) and mixed 1, 2 order model (MOE) equations have been recommended for modelling the adsorption kinetics at the interface of solid/solution. These models are mainly three-parametric equations. These new models are expected to describe the performance of a given biosorbent more accurately and to help to gain insight in biosorption mechanism (Qiu et al. 2009).

The prior kinetic models of adsorption at the interface of solid/solution can be generalized by taking into consideration the fractal-like methodology i.e., time dependence of adsorption rate coefficient. A physical significance of the concept of fractal-like has been considered for adsorption kinetics on solid surfaces that is heterogeneous energetically. The fractal-like study demonstrates that the kinetics of adsorption at interface of the solid/solution in a real system with various kinds of surface sites and with various affinities for adsorption can be demarcated by a fractal-like methodology. Based on this study, the history of process can impact the process; besides, the achieved rate coefficient of adsorption is a function of time. Some kinetic models for single-solute systems are listed in Table 1. The details of kinetic equations are provided with the Supplementary Material.

Adsorption mechanistic modelling

The removal of adsorbate species from the liquid by the solid phase takes place in three successive steps as follows (McKay et al. 1981; Singh and Pant 2006; Al-Degs et al. 2008). The three stages tangled in the mechanism of biosorption process are as follows:

1. First, the adsorbate mass transfer from the aqueous phase on the biosorbent surface, i.e., film diffusion or surface diffusion takes place;

Table 1 Adsorption kinetic models

Sr. no.	Expression	Equation form	Remarks
1	Fractional power model (FPM)	$q_t = k_{FP} t^v$	Based on adsorption capacity
2	Pseudo first-order model (PFOM)	$q_t = q_e(1 - \exp(-k_{PFO}t))$	Based on adsorption capacity
3	Pseudo second-order model (PSOM)	$q_t = \frac{(q_e^2 k_{PSO})t}{1+(q_e k_{PSO}t)}$	Chemisorption and based on adsorption capacity and chemisorption
4	Elovich model (EVM)	$q_t = \left(\frac{2.3}{b_E}\right) \times \log\left(\frac{t+1}{a_E b_E}\right) - \left(\frac{2.3}{b_E}\right) \times \log\left(\frac{1}{a_E b_E}\right)$	
5	Avrami model (AKM)	$q_t = q_e(1 - \exp[-(k_{AV}t)]^n AV)$	Multiple kinetic orders
6	Modified second-order model (MSOM)	$q_t = q_e\left\{1 - \left[\frac{1}{\beta_{2R}+k'_{2R}t}\right]\right\}$	Number of surface sites is two
7	Ritchie second-order model (RSOM)	$q_t = q_e\left\{1 - \left[\frac{1}{1+k''_{2R}t}\right]\right\}$	Adsorbent surface coverage is presumed to be zero
8	Exponential kinetic model (EXPM)	$q_t = q_e(\ln[2.72 - 1.72\ \exp(-k'_{EXP}t)])$	Exponential form of kinetic equation
9	Mixed 1, 2 order model (MOEM)	$q_t = q_e\frac{1-\exp(-k_{MOE}t)}{1-f_2\exp(-k_{MOE}t)}$	A combined form of pseudo first- and second-order equations
10	Fractal-like mixed 1, 2 order model (FMOEM)	$q_t = \frac{q_e[1-\exp(-k'_{1,0}t^\alpha)]}{1-f_{eq}\exp(-k'_{1,0}t^\alpha)}$	Time dependency of the rate coefficient
11	Fractal-like pseudo first-order model (FPFOM)	$q_t = q_e(1 - \exp(-k'_{FPFO}t^\alpha))$	Time dependency of the rate coefficient
12	Fractal−like pseudo second-order (FPSOM)	$q_t = \frac{q_e^2 k'_{FPSO}t^\alpha}{1+k'_{PSO}q_e t^\alpha}$	Time dependency of the rate coefficient
13	Fractal-like exponential (FEXPM)	$q_t = q_e\ln\left[2.72 - 1.72\exp\left(-k'''_{Exp}t^\alpha\right)\right]$	Time dependency of the rate coefficient
14	Brouser–Weron–Sotolongo model (BWSM)	$q_t = q_e\left[1 - \left(1 + (n_{BWS}-1)\left(\frac{t}{\tau_{n_{BWS} \cdot \alpha}}\right)^\alpha\right)^{-1/\left(n_{BWS-1}\right)}\right]$	Complex nature of adsorption

2. Second, internal diffusion of adsorbate via either a pore diffusion model or homogeneous solid phase diffusion model, i.e., particle diffusion occurs; and

3. The third stage is the biosorption of adsorbate on the surface sites. Due to its very fast nature, it cannot be considered for the rate-determining step.

So as to know the rate-controlling step, the following different models were applied using the experimental data of kinetic study. Some mechanistic models for single-solute systems are listed in Table 2. The details of mechanistic model equations are provided with the Supplementary Material.

Adsorption thermodynamic modelling

The entropy and Gibbs free energy parameters should be measured with the intention of deciding if the processes will happen spontaneously. Thermodynamic parameters, for example, ΔG^0, ΔH^0 and ΔS^0, can be calculated utilizing equilibrium constant while the temperature varies (Table 3), and their evaluation gives an insight into the possible nature of adsorption. The details of thermodynamic model equations are provided with the Supplementary Material.

Adsorption activation energy

The adsorption activation energy (E_a) was calculated by considering the equilibrium constants under the different experimental conditions (Table 3). The detailed equation is provided with Supplementary Material.

Results and discussion

Effect of contact time

Figure 1 exhibits the effect of contact time on the % removal of As(III) and As(V). The time required to achieve equilibrium for both As(III) and As(V) biosorption on TW/MnFe$_2$O$_4$ composite was 120 min. With further increase in time, no significant increase was achieved in removing

Table 2 Adsorption mechanistic models

Sr. no.	Expression	Equation form	Remarks
1	Weber and Morris model	$q_t = k_{int} t^{0.5} + c_{int}$	Intra-diffusion
2	Rate-limiting step	$\ln\left(1 - \frac{q_t}{q_e}\right) = \ln\frac{6}{\pi^2} - \left(\frac{D_2 \pi^2}{r^2} t\right)$	Based on diffusion
3	Dumwald–Wagner model	$\log(1 - F^2) = \frac{-K_{DW}}{2.303} t$	Intra-diffusion
4	Richenberg model	F values >0.85 $B_b t = -0.4977 - \ln(1 - F)$	Based on diffusion
		F values <0.85 $B_b t = \left(\sqrt{\pi} - \sqrt{\pi - \frac{\pi^2 F}{3}}\right)$	
5	McKay plot	$\ln(1 - F) = -K_M t$	Film diffusion
6	Bangham's model	$\log\left[\log\left(\frac{C_0}{C_0 - q_t m}\right)\right] = \log\left(\frac{K_b m}{2.303V}\right) + \alpha_b \log(t)$	Intra-diffusion
7	Diffusion coefficient	$t_{(1/2)} = \frac{0.030 r^2}{D_p}$	Based on diffusion
		$t_{(1/2)} = \frac{0.230 r \delta}{D_f} \times \frac{C_s}{C_e}$	
8	Diffusivity model	$F = 1 - \left(\frac{6}{\pi^2}\right) \sum_{m_b}^{1} \left(\frac{1}{m_b^2}\right) \exp\left(\frac{D_e t \pi^2 m_b^2}{r^2}\right)$	Chemisorption

Table 3 Thermodynamic equations and their parameters

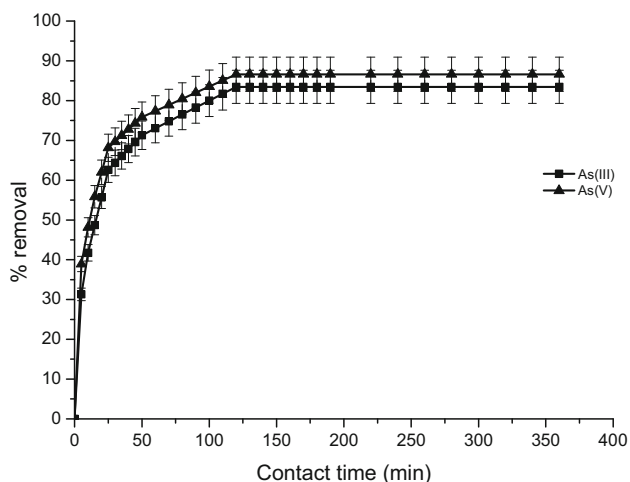| Sr. no.	Expression	Equation form	Remarks
1	Gibbs free energy	$\Delta G^0 = RT \ln K_d$ where $k_d = \frac{q_e}{c_e}$	Free energy change
2	van't Hoff	$\ln(k_d) = -\frac{\Delta H^0}{RT} + \frac{\Delta S^0}{R}$ where $k_d = \frac{q_e}{c_e}$	Enthalpy change
			Entropy change
3	Arrhenius	$\ln k_{pso} = -\frac{E_a}{RT} + \ln A$	Apparent activation energy

Fig. 1 Effect of contact time on As(III) and As(V) removal [C_0: 50 mg/L; T: 30 °C; pH: 7.0 (As(III)) and 4.0 (As(V)); M: 2 g/L)] (*error bars* represent means ± standard errors from the mean of duplicate experiments)

arsenic. So, further biosorption studies were done for a contact time of 120 min.

From the results, it is further noticeable that in all the systems, the time for saturation does not depend on the adsorbate concentration in the solution. The change in the

removal rate might be due to the fact that, initially, all biosorbent sites are readily available as well as the concentration gradient of adsorbate is very high. At optimum pH, the rapid kinetics of interaction of biosorbent–adsorbate might be obvious to increase the availability of the active sites of the biosorbent. Then, the removal of adsorbate was fast in the initial stages and gradually decreases with the interval of time till equilibrium in each case. So, the curves obtained were single, smooth and continuous approaching to equilibrium and suggested the probability of monolayer coverage of the adsorbate on the biosorbent surface (Ranjan et al. 2009).

The highest removal of As(V) ions was attained in 80 min and 60 min on *Salvadora persica* stem ash obtained at 300 °C and *Salvadora persica* stem ash obtained at 500 °C, respectively (Mostafapour et al. 2013). The highest As(III) removal of 82.23% was found at a contact time of 90 min using banana peel (condition: optimized pH 7.0, dose of 8 g/L, temperature of 35 °C and 10 mg/L As(III) ion concentration) by Kamsonlian et al. (2012a).

Biosorption kinetic studies

Information on the kinetics of adsorbate uptake is significant for indicating optimum operating conditions for full-scale batch process. As a non-linearisable kinetic model

and with the goal of comparing its fitting ability to the previous considered models, a non-linear regression analysis was done to 14 adsorption kinetic model. Table 4 shows the values of kinetic constants of all the models for the adsorption of both As(III) and As(V) by TW/MnFe$_2$O$_4$ composite. The results showed that there was no remarkable relationship between the kinetic data for both As(III) and As(V) (Fig. 2) with low correlation coefficients and high error values signifying that these models (fractional power, pseudo first-order, Elovich and exponential) are not appropriate in the present case.

In case of As(III), on the basis of maximum correlation coefficients (R, R^2 and $\overline{R^2}$), the superior and perfect fitting of the experimental results was observed employing Brouser–Weron–Sotolongo (Fig. 2) among all the verified kinetic models, whereas on the basis of the lowest error values (SSE, reduced χ^2 and root-MSE), the better and perfect demonstration of the experimental results was achieved using Ritchie second-order model (Fig. 2) among all the well-known kinetic models.

Brouers–Weron–Sotolongo model (Fig. 2) exhibited the best fit among all the models in case of As(V) in terms of the lowest error values (SSE, reduced χ^2 and root-MSE) and the highest correlation coefficients (R, R^2 and $\overline{R^2}$).

The vital supposition of Ritchie second-order model was that one adsorbate was adsorbed on two surface sites. It was supposed that the pre-adsorbed stage occurred on the TW/MnFe$_2$O$_4$ composite adsorption (Cheung et al. 2001). The biosorbent surface coverage has been typically presumed to be zero.

Going to the theory beyond the best fitting model (i.e., BWS), the adsorption phenomenon of As(V) on TW/MnFe$_2$O$_4$ composite would be governed by chemisorption interactions type, exhibiting that the rate-governing step might be chemical adsorption involving valency forces through sharing or exchange of electrons between As(V) anions and TW/MnFe$_2$O$_4$ composite. Furthermore, the BWS model conveys another interesting data which is the time significant to adsorb half the maximum amount ($\tau_{nBWS,\alpha}$). As presented in Table 4, with respect to initial arsenic concentration, 21.16453 min and 17.33022 min (lowest value) were enough for TW/MnFe$_2$O$_4$ composite to achieve half of the As(III) and As(V) uptake capacities, respectively, which is important as well as valuable parameter for computing the reaction speed. As for BWS model itself, it has a good fitting behaviour, and more implicitly, it conveys such quality data (i.e., adsorption capacity nearest to experimental value, $q_{e(BWS)}$, and the time of half reaction, $\tau_{nBWS,\alpha}$) which are very esteemed aimed at industrial treatment design purposes (Ncibi et al. 2014).

Based on good correlation coefficient (R, R^2 and $\overline{R^2}$) and low error values (SSE, reduced χ^2 and root-MSE), it can be

concluded that other kinetic models, for instance, pseudo second-order, Avrami, modified second-order, Ritchie second-order, fractal-like pseudo first-order, fractal-like pseudo second-order and fractal-like mixed 1, 2 order, fractal-like exponential models also showed good fitting of adsorption kinetic data for both As(III) and As(V) on TW/MnFe$_2$O$_4$ composite.

The value of good correlation coefficients (R, R^2 and $\overline{R^2}$) and low error values (SSE, reduced χ^2 and root-MSE) for pseudo second-order model forecasts that mechanism of biosorption/bioaccumulation is chemisorption type.

Avrami exponent (n_{AV}) [0.62816 for As(III) and 0.56394 for As(V)] is a fractionary number connected with the possible variations of the biosorption mechanism that happen all over the biosorption process (Vaghetti et al. 2009). In place of following only an integer-kinetic order, the mechanism of biosorption could follow multiple kinetic orders that are altered throughout the contact of the adsorbate with TW/MnFe$_2$O$_4$ composite (Vaghetti et al. 2009). n_{AV} is a resultant of the multiple kinetic order of the biosorption procedure.

It is understood that the mixed 1, 2-order rate equation is linear in the Lagergren coordinates (i.e., it behaves like the first-order equation) near to the equilibrium and somewhat in the initial portion of the experiment. Precisely, we may conclude that it contains two linear segments connected with a curved one. Actually, the second-order equation shows linear behaviour in the initial portion of the experiment also, though the linear section is quite short. On the other hand, MOE may be treated as Langmuir equation for energetically homogeneous surfaces or as purely empirical equation for energetically heterogeneous surfaces.

The vital assumption of modified second-order model was that a number of surface sites, n_R, are used by each adsorbate. It was supposed that the pre-adsorbed stage occurred on TW/MnFe$_2$O$_4$ composite biosorption.

In case of fractal-like models (fractal-like pseudo first-order, fractal-like pseudo second-order, fractal-like exponential, and fractal-like mixed 1, 2 order), the biosorption rate coefficient is considered a function of time using the fractal-like idea. One of the probable physical significances of fractal-like kinetics was that the biosorption of As(III) and As(V) occurred at solid/solution interface. In this approach, it was showed that by passing time, various paths for biosorption of As(III) and As(V) on surface appear (Haerifar and Azizian 2012).

Final remarks on biosorption kinetic studies

The value of correlation coefficient (R, R^2 and $\overline{R^2}$) for Brouers–Weron–Sotolongo model was better than acquired using the other kinetic model for As(III). But on the basis of

Table 4 Kinetic constants of studied models for As(III) and As(V) biosorption onto TW/MnFe$_2$O$_4$ composite

Kinetic models	Parameters	Values for As(III)	Values for As(V)
Fractional power	k_{FP} (mg/g min)	9.1429	10.69144
	v	0.1557	0.13343
	Reduced χ^2	1.88984	1.52499
	SSE	58.58498	47.27481
	R	0.95687	0.96392
	R^2	0.9156	0.92914
	$\overline{R^2}$	0.91288	0.92685
	Root-MSE	1.37471	1.23491
Pseudo first-order	k_{PFO} (1/min)	0.05559	0.06876
	$q_{e(PFO)}$ (mg/g)	20.41584	21.0985
	Reduced χ^2	0.86792	1.13152
	SSE	26.90562	35.07705
	R	0.98043	0.97336
	R^2	0.96124	0.94742
	$\overline{R^2}$	0.95999	0.94573
	Root-MSE	0.93162	1.06373
Pseudo second-order	$q_{e(PSO)}$ (mg/g)	21.94934	22.46476
	k_{PSO} (g/mg min)	0.00418	0.00531
	Reduced χ^2	0.14054	0.15217
	SSE	4.35669	4.71725
	R	0.99686	0.99646
	R^2	0.99372	0.99293
	$\overline{R^2}$	0.99352	0.9927
	Root-MSE	0.37488	0.39009
Elovich	a_E (mg/g min)	18.99018	50.14515
	b_E (g/mg)	0.34157	0.37838
	Reduced χ^2	1.19885	1.02668
	SSE	37.16432	31.82697
	R	0.97286	0.97585
	R^2	0.94646	0.95229
	$\overline{R^2}$	0.94474	0.95075
	Root-MSE	1.09492	1.01325
Avrami	k_{AV} (1/min)	0.05629	0.07217
	$q_{e(Avrami)}$ (mg/g)	21.08249	21.88802
	n_{AV}	0.62816	0.56394
	Reduced χ^2	0.07185	0.06326
	SSE	2.15556	1.89777
	R	0.99845	0.99858
	R^2	0.99689	0.99716
	$\overline{R^2}$	0.99669	0.99697
	Root-MSE	0.26805	0.25151

Table 4 continued

Kinetic models	Parameters	Values for As(III)	Values for As(V)
Modified second-order	$q_{e(MSO)}$ (mg/g)	21.9671	22.48469
	β_{2R}	1.01159	1.01614
	k'_{2R} (1/min)	0.0907	0.1175
	Reduced χ^2	0.14287	0.15279
	SSE	4.28605	4.58363
	R	0.99691	0.99656
	R^2	0.99383	0.99313
	$\overline{R^2}$	0.99341	0.99267
	Root-MSE	0.37798	0.39088
Ritchie second-order	$q_{e(Ritchie)}$ (mg/g)	14.37448	22.46465
	k''_{2R} (1/min)	0.10302	0.11919
	Reduced χ^2	0.06059	0.15217
	SSE	1.87839	4.71725
	R	0.99679	0.99646
	R^2	0.99359	0.99293
	$\overline{R^2}$	0.99338	0.9927
	Root-MSE	0.24616	0.39009
Exponential	k_{EXP} (mg/g min)	2.01319163	1.053717856
	$q_{e(EXP)}$ (mg/g)	21.94932	21.23147
	Reduced χ^2	0.48065	0.69605
	SSE	14.90018	21.57749
	R	0.98921	0.9837
	R^2	0.97854	0.96766
	$\overline{R^2}$	0.97784	0.96661
	Root-MSE	0.69329	0.83429
Mixed 1, 2 order	k_{MOE} (1/min)	0.00929	0.00475
	$q_{e(MOE)}$ (mg/g)	21.20349	22.09592
	f_2	0.89836	0.96051
	Reduced χ^2	0.13192	0.15649
	SSE	3.95755	4.69477
	R	0.99715	0.99648
	R^2	0.9943	0.99296
	$\overline{R^2}$	0.99392	0.99249
	Root-MSE	0.36321	0.39559
Fractal-like mixed 1, 2 order	$q_{e(FMOE)}$ (mg/g)	21.08342	21.88937
	f_2	0	0
	$k'_{1,0}$ (1/min)$^\alpha$	0.16434	0.22777
	$\alpha_{(FMOE)}$	0.62777	0.5633
	Reduced χ^2	0.07433	0.06547
	SSE	2.15568	1.89859
	R	0.99845	0.99858
	R^2	0.99689	0.99715
	$\overline{R^2}$	0.99657	0.99686
	Root-MSE	0.27264	0.25587

Table 4 continued

Kinetic models	Parameters	Values for As(III)	Values for As(V)
Fractal-like pseudo first-order	$q_{e(FPFO)}$ (mg/g)	21.08249	21.88931
	k'_{FPFO} (1/min)$^{\alpha}$	0.16409	0.22728
	$\alpha_{(FPFO)}$	0.62815	0.56363
	Reduced χ^2	0.07185	0.06326
	SSE	2.15556	1.8978
	R	0.99845	0.99858
	R^2	0.99689	0.99716
	$\overline{R^2}$	0.99669	0.99697
	Root-MSE	0.26805	0.25152
Fractal-like pseudo second-order	$q_{e(FPSO)}$ (mg/g)	22.1174	22.91257
	k'_{FPSO} (g/mg min)$^{\alpha}$	0.0046	0.00683
	$\alpha_{(FPSO)}$	0.95743	0.88236
	Reduced χ^2	0.14102	0.12574
	SSE	4.23067	3.77215
	R	0.99695	0.99717
	R^2	0.99391	0.99435
	$\overline{R^2}$	0.9935	0.99397
	Root-MSE	0.37553	0.3546
Fractal-like exponential	$q_{e(FEXP)}$ (mg/g)	21.0674	21.86688
	k''_{EXP} (1/min)$^{\alpha}$	0.065463593	0.085096781
	$\alpha_{(FEXP)}$	0.72168	0.65009
	Reduced χ^2	0.07179	0.06377
	SSE	2.15362	1.91312
	R	0.99845	0.99857
	R^2	0.9969	0.99713
	$\overline{R^2}$	0.99669	0.99694
	Root-MSE	0.26793	0.25253
Brouser–Weron–Sotolongo	$\tau_{nBWS,\alpha}$ (min)	21.16453	17.33022
	$q_{e(BWS)}$ (mg/g)	20.94439	21.72236
	n_{BWS}	0.79892	0.76752
	$\alpha_{(BWS)}$	0.55111	0.48026
	Reduced χ^2	0.06786	0.05609
	SSE	1.96785	1.62665
	R	0.99858	0.99878
	R^2	0.99717	0.99756
	$\overline{R^2}$	0.99687	0.99731
	Root-MSE	0.26049	0.23684

the acquired error values (SSE, reduced χ^2 and root-MSE), the Ritchie second-order model exhibited the best fit to the biosorption kinetic data of As(III) among all the models. The value of correlation coefficient (R, R^2 and $\overline{R^2}$) and error values (SSE, reduced χ^2 and root-MSE) for Brouers–Weron–Sotolongo kinetic model was better than that observed utilizing the other kinetic models for As(V). So, the kinetics of As(III) and As(V) biosorption using TW/MnFe$_2$O$_4$ composite as a biosorbent can be well clarified by Brouers–Weron–Sotolongo kinetic model. It signifies that the mechanism of

biosorption of both As(III) and As(V) is complex. The complex phenomenon of biosorption may include chemical interactions between the adsorbate and the functional groups on the biosorbent surface, which may involve hydrogen bounding, ligand exchange, Van der Waals, electrostatic interactions and hydrophobic interactions.

Among the models, pseudo second-order model also possessed a good fitness with experimental kinetic data. This tendency comes as a suggestion that the rate-limiting steps in biosorption of arsenic (either As(III) or As(V)) are
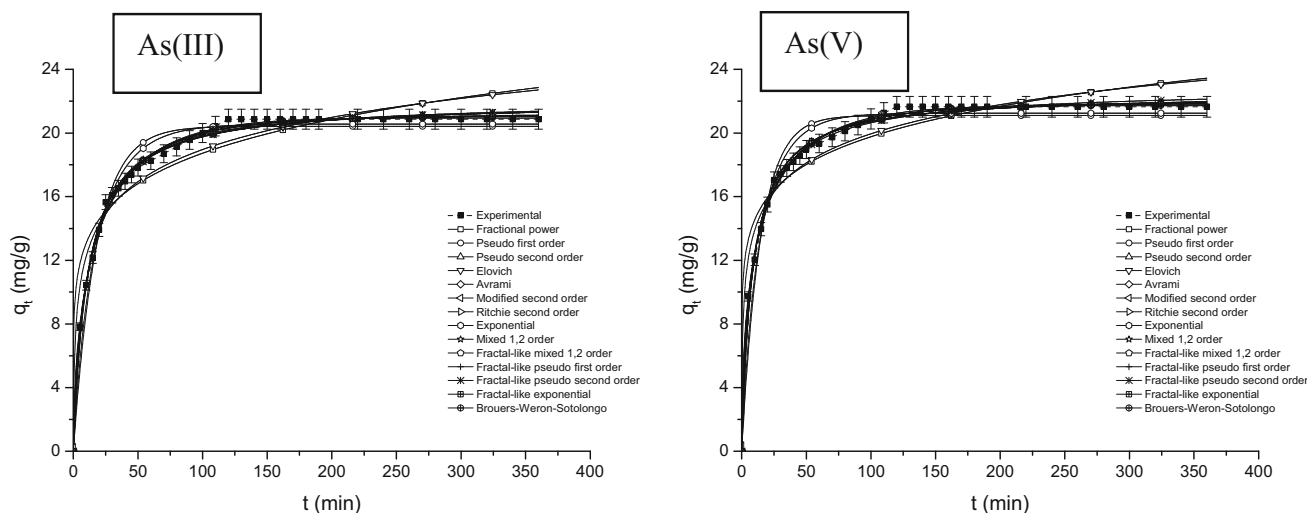
Fig. 2 Kinetic modelling of As(III) and As(V) biosorption on the TW/MnFe$_2$O$_4$ composite [t: 0–360 min; C_0: 50 mg/L; M: 2 g/L; pH: 7.0 (As(III)) and 4.0 (As(V)); T: 30 °C] (*error bars* represent means $\pm$ standard errors from the mean of duplicate experiments)

chemisorption involving valence forces through the sharing or exchange of electrons between TW/MnFe$_2$O$_4$ composite and arsenic (either As(III) or As(V)) ions (Miretzky et al. 2008), complexation, coordination and/or chelation (Lu and Gibb 2008).

It is vital to obtain the rate at which As(III) or As(V) is adsorbed on the surface of TW/MnFe$_2$O$_4$ composite that is significant for designing fixed-bed biosorption column. Using the biosorption rate, kinetic constants are calculated to determine the equilibrium capacity of biosorbent and mass transfer coefficient at various aqueous phase concentrations. Amount of As(III) or As(V) biosorbed on solid surface is calculated using the kinetic equation which is vital for esteeming the concentration of the aqueous phase in fixed-bed column operation. The main design factors of fixed-bed adsorption column, the breakthrough time as well as the shape of breakthrough curve are dependent on adsorption rate. For the quicker adsorption rate, breakpoint time is attained prior; besides, the breakthrough curve shape is steeper.

The descriptive models from the best to worst for As(III) and As(V) were sorted according to GoFM values and shown in Table S1 and Table S2, respectively.

Consequently, at this point, the fitting "ambiguity" influenced by the correlation coefficient (R, R^2 and $\overline{R^2}$) and error values (SSE, reduced χ^2 and root-MSE) was for As(III), as the correlation coefficient (R, R^2 and $\overline{R^2}$) confirmed Brouers–Weron–Sotolongo as the best fitting model (the highest correlation coefficient) whereas the error values (SSE, reduced χ^2 and root-MSE) showed that the Ritchie second-order model is the best (the lowest error values). Thus, for overcoming this doubt, it would be modest and practical for comparing the theoretically assessed q_e values

with the experimental ones. According to correlation coefficient $\overline{R^2}$ values, the fitness of the models for all kinetic models is almost equivalent to each other for As(III). So, based on equivalent adsorption capacity, the orders followed by the models in declining manner are informed in Table S3 of Supplementary Materials. From the Table S3 of Supplementary Materials, it can be concluded that on the basis of equivalent biosorption capacity, Ritchie second-order model and fractal-like pseudo second-order kinetic models are the best fitting models for As(III) and As(V), respectively, owing to the highest value.

Biosorption mechanistic studies

Intraparticle diffusion model

Results of intraparticle model for both As(III) and As(V) are given in Table 5. Figure 3 indicated the multi-linear nature of intraparticle model. Since the plot did not pass through the origin, intraparticle diffusion was not the solely rate-governing step. So, there were three processes controlling the rate of biosorption; however, only one was rate-controlling in any certain time range. The intraparticle diffusion rate constant k_{int2} for both As(III) and As(V) was valued from the slope of the second linear portion (Fig. 3; Table 5). The multi-linear curve of the intraparticle model with intercept C_{int2} specified the fact that both intraparticle diffusion of adsorbate through the mesoporus openings filled with liquid and film/external mass transfer across the thickness of boundary layer were the rate-governing steps in the biosorption of both As(III) and As(V) kinetics on the surface of TW/MnFe$_2$O$_4$ composite. The value of intercept C_{int} obtained through the model provided the value of

Table 5 Mechanistic constants of studied models for As(III) and As(V) biosorption onto TW/MnFe$_2$O$_4$ composite

Mechanistic models	Parameters	Values for As(III)	Values for As(V)
Intraparticle diffusion model	k_{int1} (mg/g min$^{0.5}$)	3.08224	3.3528
	C_{int1} (mg/g)	0.37134	0.90435
	k_{int2} (mg/g min$^{0.5}$)	0.85287	0.75446
	C_{int2} (mg/g)	11.53739	13.39846
	$\overline{R_1^2}$	0.99483	0.97724
	$\overline{R_2^2}$	0.99518	0.99518
Determination of rate-limiting step	D_1 (cm^2/s)	1.99205E−05	1.74369E−05
	D_2 (cm^2/s)	9.68082E−06	9.7479E−06
Dumwald–Wagner model	k_{DW} (1/min)	0.02800448	0.025333
	$\overline{R^2}$	0.97582	0.96762
Richenberg model	$\overline{R^2}$	0.9708	0.9702
McKay plot	k_{M1} (1/min)	0.05143	0.05678
	k_{M2} (1/min)	0.02585	0.02585
	$\overline{R_1^2}$	0.9693	0.94985
	$\overline{R_2^2}$	0.94785	0.94785
Bangham's model	k_b (L/g)	9.58747	30.41613
	α_b	0.47134	0.25224
	$\overline{R^2}$	0.98276	0.96952
Diffusion coefficient	D_p (cm^2/s)	1.39587E−07	1.72657E−07
	D_f (cm^2/s)	1.09785E−07	1.67623E−07
Diffusivity	D_e (m^2/s)	8.80E−14	9.10E−14
	$\overline{R^2}$	0.97114	0.97053
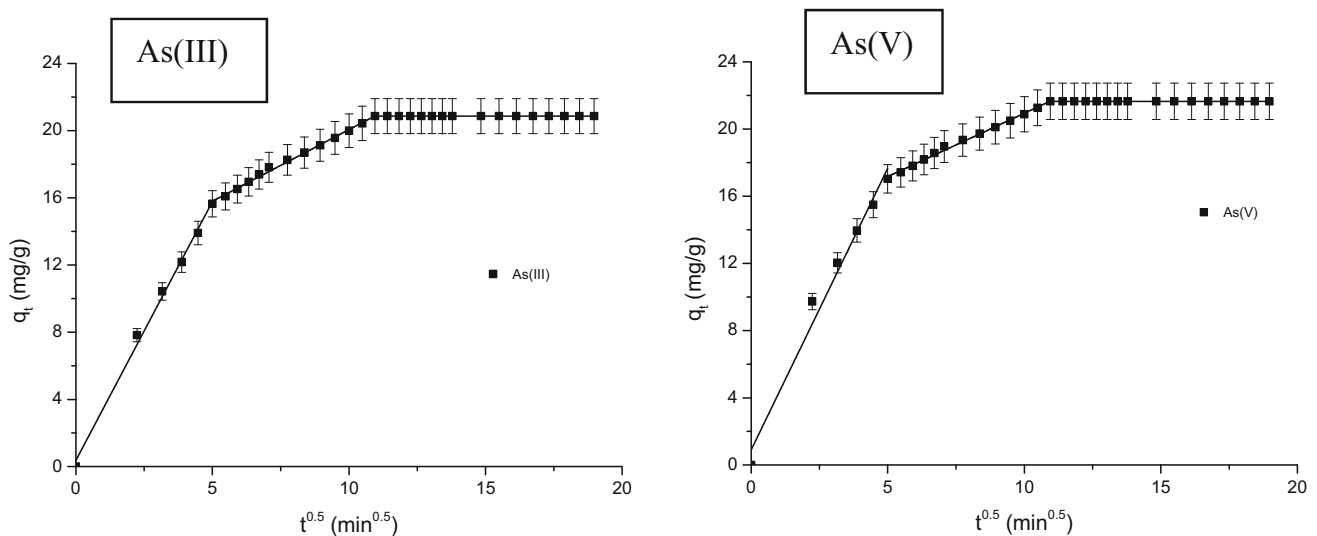
Fig. 3 Intraparticle diffusion modelling of As(III) and As(V) biosorption onto the TW/MnFe$_2$O$_4$ composite [t: 0–360 min; C_0: 50 mg/L; M: 2 g/L; pH: 7.0 (As(III)) and 4.0 (As(V)); T: 30 °C] (*error bars* represent means ± standard errors from the mean of duplicate experiments)

thickness of boundary layer of liquid surrounding the composite (Kavitha and Namasivayam 2007).

The interpretation of the discrete data points seen in Fig. 3 and Table 5 specified that intraparticle mechanistic model had been appropriate to cost-effectively and expertly

describe the biosorption of both As(III) and As(V) on the surface of TW/MnFe$_2$O$_4$ composite in terms of linear regression coefficient adjusted R-square ($\overline{R^2}$), ranging between 0.97724 and 0.99518 in both the cases. Larger value of intercepts attained for second linear portion, i.e.,

C_{int2}, suggested that the film diffusion had played a superior role as the rate-limiting step (Rengaraj et al. 2007).

Determination of rate-limiting step

The values of the film diffusion coefficient D_1 and the pore diffusion coefficient D_2 for both As(III) and As(V) are given in Table 5. The high negative exponential of almost closest value specified that both pore diffusion and film diffusion had controlled the mechanism of biosorption for both As(III) and As(V).

Dumwald–Wagner model

The plot (Fig. 4) of $\log(1 - F^2)$ versus t has yielded almost perfect linear curves for the removal of both As(III) and As(V) by TW/MnFe$_2$O$_4$ composite, respectively, but did not pass through the origin indicating that the diffusion of adsorbate into pores of the biosorbent was not the solely rate governing-step in both the cases. Table 5 lists the computed results of Dumwald–Wagner model. In the current study, the linearity of the plots intersected the origin of coordinates; so, film diffusion process was the rate-controlling step.

Richenberg model or Boyd plot

The results of the corresponding model for both As(III) and As(V) are exhibited in Table 5 and Fig. 5, respectively. From the plots of $B_b t$ versus t, it was found that the plots had vital linear form for both As(III) and As(V) at studied temperature but did not pass through origin which had selected the ongoing biosorption processes to be governed by film diffusion mechanism.

Film diffusion mass transfer rate equation or McKay plot

The values gained for $\ln(1 - F)$ as a function of time t, were plotted in Fig. 6 for As(III) and As(V), respectively, and the results of the respective model for both As(III) and As(V) are exhibited in Table 5. The rate constant of the initial quick process (k_{M1}) was evaluated from the slope of the first straight line (Fig. 6). As can be understood from Fig. 6, the rate constant of the sluggish process (k_{M2}) was attained from the slope of the second linear portion. It is noticeable that the initial rapid process was controlled by film diffusion. Also, the values of k_{M2} are smaller than the values of k_{M1} for both As(III) and As(V). Thus, the found values of k_{M2} were evidence of a pore diffusion mechanism in the second stage of the biosorption (Atun and Hisarli 2003). The presence of two straight lines for both As(III) and As(V) indicated that two processes, i.e., film diffusion and pore diffusion are involved.

The plots were nearly linear for both As(III) and As(V), but it did not return perfect linearity. Therefore, pore diffusion was not the rate-controlling step. In the prevailing system, film diffusion was the rate-governing step.

Bangham's model

The results of the respective model for both As(III) and As(V) are shown in Table 5 and (Fig. 7). The goodness-of-fit of curve for Bangham's model was related in terms of correlation coefficient adjusted R-square ($\overline{R^2}$). Values of Bangham parameters k_b and α are 9.58747 L/g and 0.47134 for biosorption of As(III) and 30.41613 L/g and 0.25224 for biosorption of As(V) with correlation coefficients of 0.996 and 0.984, respectively. The double logarithmic plot
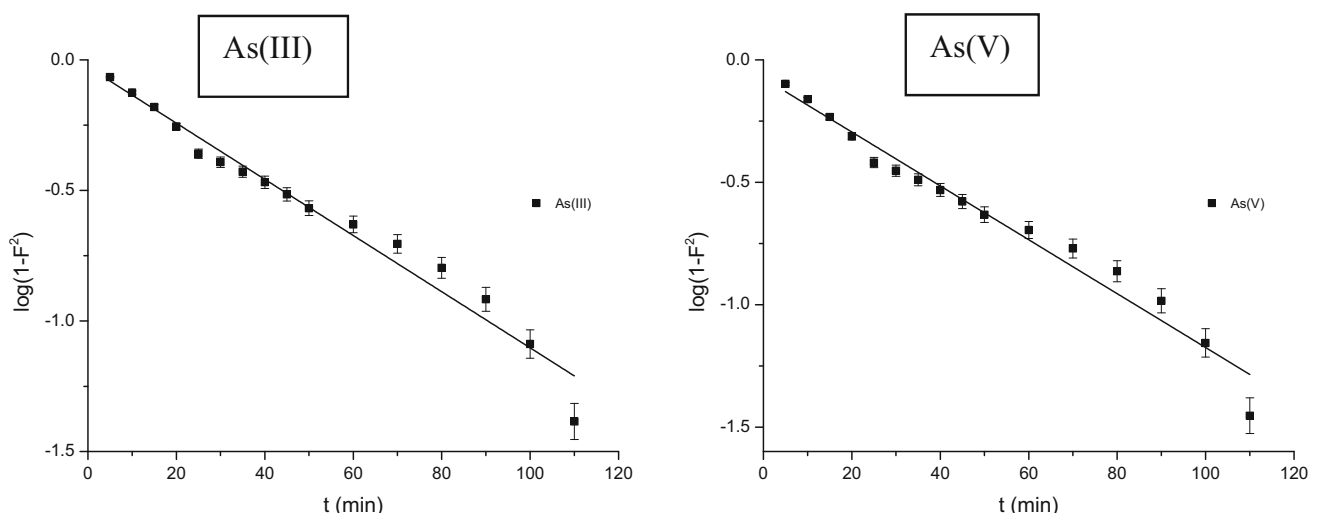

Fig. 4 Dumwald–Wagner modelling of As(III) and As(V) biosorption on the TW/MnFe$_2$O$_4$ composite [t: 0–360 min; C_0: 50 mg/L; M: 2 g/L; pH: 7.0 (As(III)) and 4.0 (As(V)); T: 30 °C] (*error bars* represent means ± standard errors from the mean of duplicate experiments)
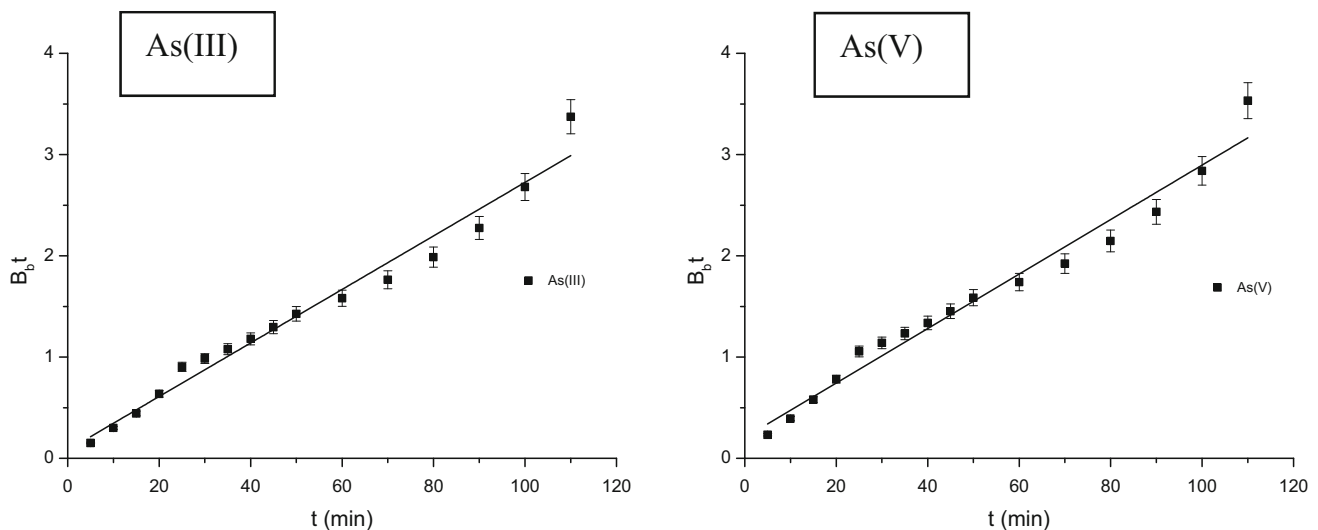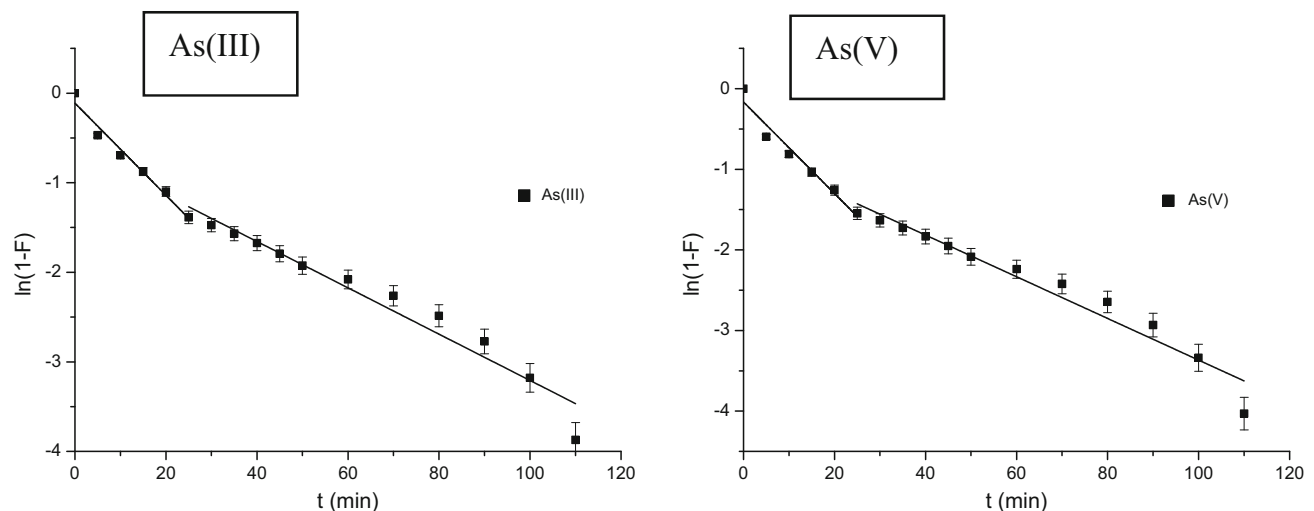
Fig. 5 Richenberg modelling of As(III) and As(V) biosorption on the TW/MnFe$_2$O$_4$ composite [t: 0–360 min; C_0: 50 mg/L; M: 2 g/L; pH: 7.0 (As(III)) and 4.0 (As(V)); T: 30 °C] (*error bars* represent means ± standard errors from the mean of duplicate experiments)

Fig. 6 McKay plot of As(III) and As(V) biosorption on the TW/MnFe$_2$O$_4$ composite [t: 0–360 min; C_0: 50 mg/L; M: 2 g/L; pH: 7.0 (As(III)) and 4.0 (As(V)); T: 30 °C] (*error bars* represent means ± standard errors from the mean of duplicate experiments)

(Fig. 7) for both As(III) and As(V), as specified by above equation, did not return perfect linear curves, and some data were discrete for the removal of As(III) and As(V) by TW/MnFe$_2$O$_4$ composite enlightening that the diffusion of adsorbate within pores of the biosorbent was not solely the rate-governing step (Weber and Morris 1963), and that film diffusion also had influence on the rate-limiting step.

Determination of diffusion coefficient

The D_p and D_f values for As(III) were 1.39587×10^{-7} and 1.09785×10^{-7} cm^2/s, respectively. Similarly, these values for As(V) were 1.72657×10^{-7} and 1.67623×10^{-7} cm^2/s, respectively (Table 5).

So, in the current case, pore diffusion was not the solely rate-controlling step for both As(III) and As(V). For As(III), the value of D_f (1.72657×10^{-7} cm^2/s) falls within the range of 10^{-6} and 10^{-8} cm^2/s, and for As(V), the D_f value (1.67623×10^{-7} cm^2/s) is also in the order of 10^{-7}. So, it was observed that the film diffusion had been the rate-governing step for both As(III) and As(V).

Higher value of D_f and smaller value of D_p of As(V) than that of As(III) was because of the presence of As(V) as totally positively charged species and As(III) as mostly neutral species at the experimental pH. Because of negative charge of As(V), it was willingly transported from the bulk solution to mainly the positively charged
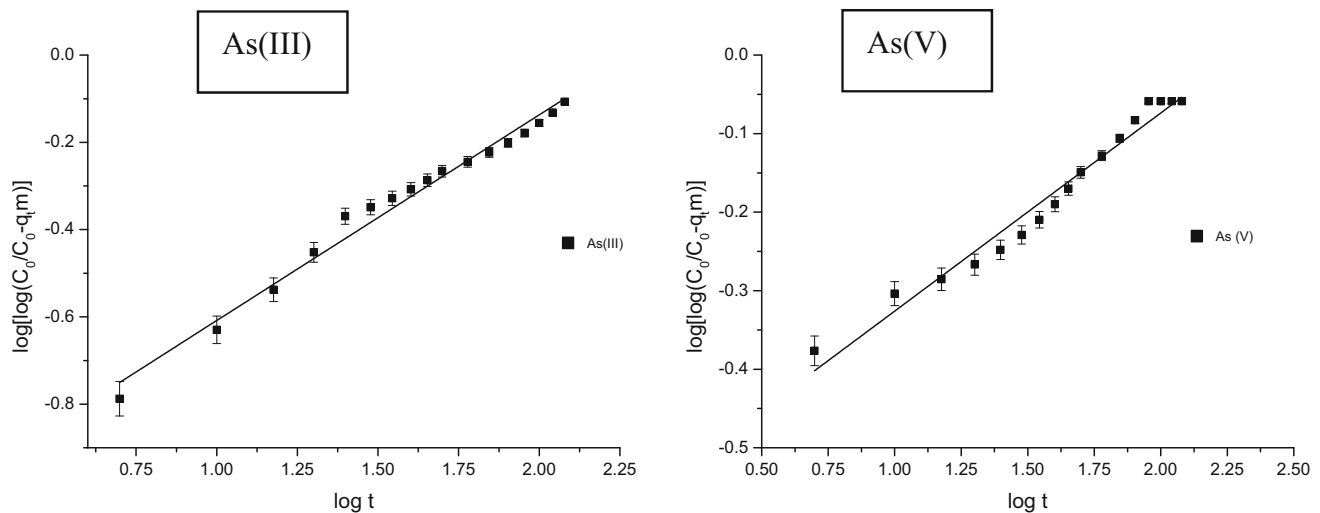
Fig. 7 Bangham modelling of As(III) and As(V) biosorption on the TW/MnFe$_2$O$_4$ composite [t: 0–360 min; C_0: 50 mg/L; M: 2 g/L; pH: 7.0 (As(III)) and 4.0 (As(V)); T: 30 °C] (*error bars* represent means $\pm$ standard errors from the mean of duplicate experiments)

biosorbent surface and got biosorbed on the active sites of biosorbent surface instead of the interior pores.

Determination of diffusivity

From the slope $\pi^2 D_e/r^2$ of the plot of $\ln[1/(1 - F^2)]$ versus t (Fig. 8; Table 5), the value of diffusion coefficient, D$_e$ as assessed, was seen to be 8.8×10^{-14} and 9.1×10^{-14} m^2/s for As(III) and As(V) biosorption on TW/MnFe$_2$O$_4$ composite, respectively. For the current systems, the value of D_e lies within the range of 10^{-9}–10^{-17} m^2/s; consequently, the system was chemisorption system. The values of the diffusion coefficient, D$_e$, fell well within the magnitudes reported in the literature (Naiya et al. 2009; Singha and Das 2011).

Final remarks on biosorption mechanistic studies

The above-considered models for biosorption of both As(III) and As(V) specified that two processes, i.e., film diffusion (diffusion of adsorbate through the solution to the external surface of biosorbent or boundary layer diffusion of adsorbate) and pore diffusion (diffusion of the adsorbate from the surface film into the pores) were involved in the present biosorption processes for both As(III) and As(V) and pore diffusion was not the solely rate-controlling step. Usually, film diffusion controlled the rate-controlling step in both the cases. The uptake of arsenic (either As(III) or As(V)) species from the liquid to the solid phase was carried out in three consecutive steps (Al-Degs et al. 2008). First, film diffusion occurred. Second, pore diffusion took place. The third step is the biosorption/bioaccumulation which is being very rapid in nature and cannot be taken into account for the rate-determining step (Singh and Pant 2006).

Effect of temperature

The temperature has two main impacts on the biosorption process. Increasing the temperature is known to increase the rate of diffusion of the adsorbate because of the reduction in the viscosity of the solution. Similarly, varying the temperature will alter the equilibrium biosorption capacity of the biosorbent for a specific adsorbate (Nouri et al. 2007).

The effect of temperature on the removal efficiency of As(III) and As(V) was carried out in the range of 20–50 °C during the equilibrium time. The results indicated that the highest removal was acquired at a temperature of 30 °C (Fig. 9). Initial increase in removal efficiency up to 30 °C is usually due to the increase in collision frequency between biosorbent and adsorbate. Further increase in temperature (>30 °C) resulted in lower removal efficiency for arsenic removal by TW/MnFe$_2$O$_4$ composite. This can be explained by the spontaneity and exothermicity of the biosorption process. This reduction in removal efficiency might be because of many factors: the relative increase in the dodging tendency of the arsenic ions from the solid biosorbent phase to the bulk liquid phase; deactivating the surface of biosorbent or destructing some active sites on the surface of biosorbent owing to bond ruptures (Meena et al. 2005; Romero-Gonzalez et al. 2005) or because of the weakening of biosorptive forces between the adsorbate species and the active sites of the biosorbents and also between the adjacent molecules of biosorbed phase for high temperatures or movement of biosorbents with higher speed; thus, lower interaction time with the biosorbent active sites was obtainable for them (Yadav and Tyagi 1987; Roy et al. 2014). Maximum removal of As(III) and As(V) was observed at 30 °C by Kamsonlian et al. (2012b)
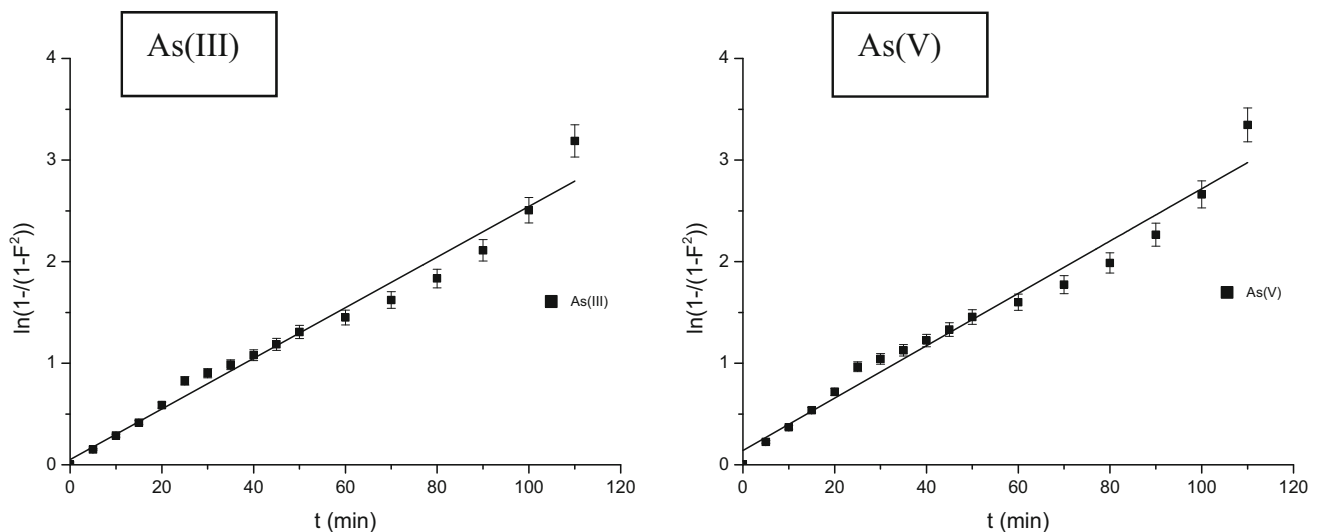
Fig. 8 Diffusivity of As(III) and As(V) biosorption on the TW/MnFe$_2$O$_4$ composite [t: 0–360 min; C_0: 50 mg/L; M: 2 g/L; pH: 7.0 (As(III)) and 4.0 (As(V)); T: 30 °C] (*error bars* represent means $\pm$ standard errors from the mean of duplicate experiments)
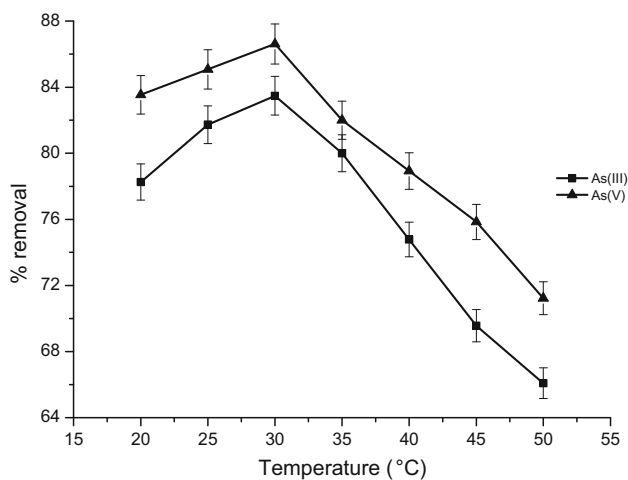

Fig. 9 Effect of temperature on As(III) and As(V) removal [C_0: 50 mg/L; pH: 7.0 (As(III)) and 4.0 (As(V)); M: 2 g/L; t: 120 min] (*error bars* represent means $\pm$ standard errors from the mean of duplicate experiments)

on powdered *Psidium guajava* (*Guava*) leaf and by Mondal et al. (2007) on GAC and GAC-Fe and also by Mondal et al. (2009) on GAC-Cu. Comparable trend was specified by Roy et al. (2014) using iron-impregnated sugarcane carbon and Saqib et al. (2013) using Blue Pine (*Pinus wallichiana*) and Walnut (*Juglans regia*).

Biosorption thermodynamic studies

The evaluated values of the thermodynamic parameters from the plot of ln k_d versus $1/T$ (Fig. 10) are presented in Table 6. The equilibrium constant k_d was evaluated, when the temperature was altered between 20 and 50 °C for both As(III) and As(V). The highest removal of adsorbate was

achieved at 30 °C in both the cases. The removal efficiency initially increased with rising the temperature from 20 to 30 °C. Then, it reduced with rising the temperature from 30 to 50 °C. The ΔH^0 values found for the biosorption of both As(III) and As(V) were negative due to the exothermic nature of the biosorption process. The value achieved for As(V) biosorption was more than the value acquired for As(III). A negative value of ΔG^0 specified the spontaneous nature of the biosorption process; nonetheless, the negative value of ΔS^0 showed a decrease in the randomness at the solid/solution interface throughout the biosorption process (Ngah and Hanafiah 2008). Higher negative value of ΔG^0 at a temperature of 30 °C, as was achieved in the study, inferred more driving force for biosorption at 30 °C (Crini and Badot 2008). The values of ΔG^0 achieved in the present study were between -18.48 to -19.73 and -19.1 to -20.36 kJ/mol for As(III) and As(V), respectively. Therefore, it indicated that the mechanism of present biosorption process had happened via ion exchange and/or surface complexation mechanism.

Effect of initial arsenic concentration on biosorption kinetics

To investigate the effect of initial concentration on kinetic studies, a series of contact time experiments for both As(III) and As(V) were conducted at various initial concentrations (50–2000 mg/L) at temperature of 30 °C. (Fig. 11) reveals that the contact time necessary for both As(III) and As(V) with initial concentration of 50–1000 mg/L for attaining equilibrium was 120 min. But for both As(III) and As(V), with higher initial concentration (>1000–2000 mg/L), higher equilibrium time of
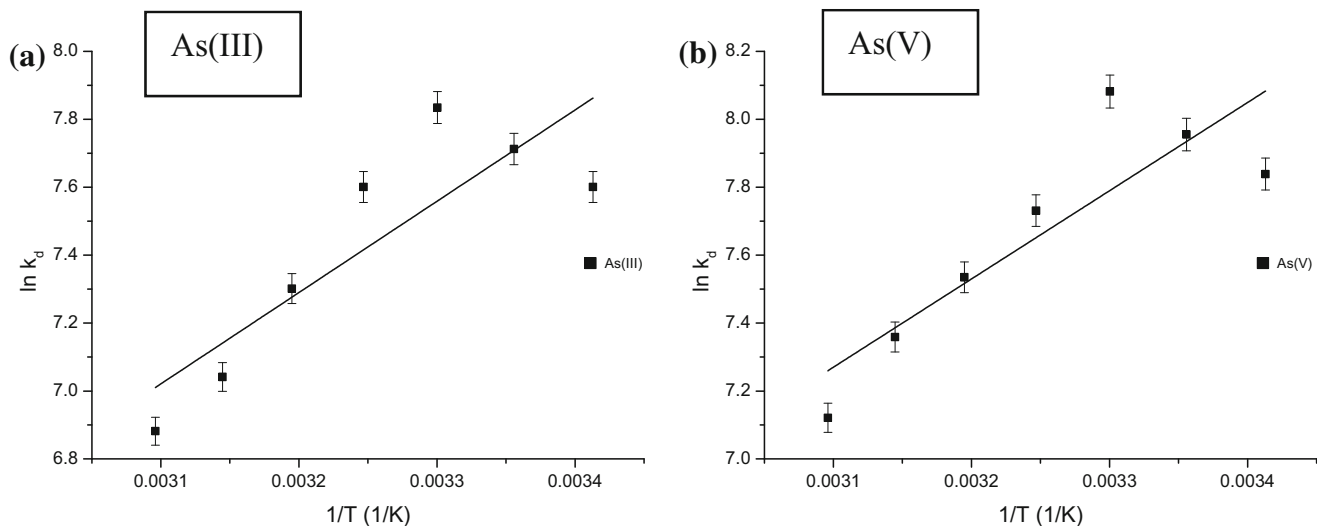
Fig. 10 Thermodynamic modelling of **a** As(III) and **b** As(V) biosorption on the TW/MnFe$_2$O$_4$ composite [T: 20–50 °C; C_0: 50 mg/L; pH: 7.0 (As(III)) and 4.0 (As(V)); M: 2 g/L; t: 120 min] (*error bars* represent means $\pm$ standard errors from the mean of duplicate experiments)

Table 6 Thermodynamic constants for As(III) and As(V) biosorption onto TW/MnFe$_2$O$_4$ composite

Inorganic form	T (K)	$-\Delta G^0$ (KJ/mol)	$-\Delta H^0$ (KJ/mol)	$-\Delta S^0$ (J/mol K)
As(III)	293	18.5158136	22.3468682	0.01090132
	298	19.1089402		
	303	19.7362616		
	308	19.4637221		
	313	19.0009773		
	318	18.6161198		
	323	18.4804829		
As(V)	293	19.0955483	21.5974793	0.00650803
	298	19.7097173		
	303	20.3596543		
	308	19.7967507		
	313	19.6079425		
	318	19.455767		
	323	19.1234984		

160 min was needed. As can be decided from Fig. 11, the amount of the biosorbed both As(III) and As(V) on the surface of TW/MnFe$_2$O$_4$ composite amended with time and, at some point in time, achieved a constant value beyond which no more As(III) or As(V) was removed from solution. At the moment, the amount of both As(III) and As(V) desorbing from the biosorbent was in a state of dynamic equilibrium with the quantity of both As(III) and As(V) being biosorbed on the surface of TW/MnFe$_2$O$_4$ composite. The time necessary for achieving this state of equilibrium is called the equilibrium time. Therefore, the rate of biosorption reduced with time till it progressively prone to a plateau because of the constant reduction in the concentration driving force. Comparable trend was described by Kamsonlian et al. (2012c) using mango leaf powder and rice husk for biosorption of As(III).

Determination of initial sorption rate

From Fig. S2 and Table 7, it is observed that the pseudo second-order rate constants (k_{PSO}) were seen to decrease and the initial sorption rates (h) were understood for increasing with increased initial concentration of both As(III) and As(V). The initial sorption rate was superior for higher initial As(III) and As(V) concentration as the resistance to uptake of both As(III) and As(V) decreased as the mass transfer driving force enhanced.

The evaluated $q_{e(PSO)}$ values just agreed satisfactorily with the experimental data, and the high correlation coefficient (R, R^2 and $\overline{R^2}$) and low error values (SSE, reduced χ^2 and root-MSE) show that the model can be used for the whole biosorption process and allowed the chemisorption of both As(III) and As(V) on TW/MnFe$_2$O$_4$ composite.
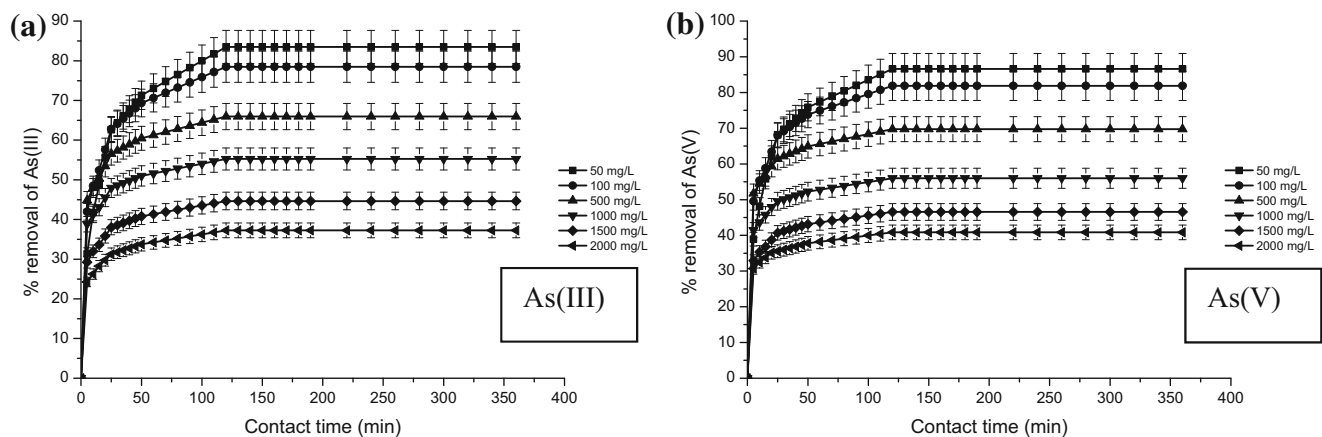
Fig. 11 Effect of initial concentration on contact time for **a** As(III) and **b** As(V) biosorption on the TW/MnFe$_2$O$_4$ composite [C_0: 50–2000 mg/L; t: 0–360 min; pH: 7.0 (As(III)) and 4.0 (As(V)); M: 2 g/L; T: 30 °C] (*error bars* represent means ± standard errors from the mean of duplicate experiments)

Table 7 Initial sorption rate for As(III) and As(V) biosorption/bioaccumulation onto TW/MnFe$_2$O$_4$ composite

Inorganic form	Concentration (mg/L)	K_{PSO} (g/mg min)	H (mg/g min)
As(III)	50	0.00531	2.679773
	100	0.00476	8.221098
	500	0.00163	44.92546
	1000	0.0011	84.76524
	1500	8.26E−04	89.36715
	2000	7.59E−04	100.308
As(V)	50	0.00531	2.679773
	100	0.00476	8.221098
	500	0.00219	66.69726
	1000	0.00137	107.7652
	1500	0.00109	127.5314
	2000	0.00102	162.0542

Effect of temperature on biosorption kinetic

Temperature is a significant factor governing the biosorption process. The effect of temperature on the biosorption of both As(III) and As(V) by TW/MnFe$_2$O$_4$ composite was done from 30 to 50 °C at C_0 is 50 mg/L and TW/MnFe$_2$O$_4$ composite loading is 2 g/L. A declining biosorption rate of both As(III) and As(V) with rising temperature from 30 to 50 °C acknowledged the process to be exothermic (Fig. 12). This is considered before concerning thermodynamic parameters in Supplementary Materials. Related trend has been defined by Roy et al. (2014) using iron-impregnated sugarcane carbon Miretzky et al. (2008) and Saqib et al. (2013) using Blue Pine (*Pinus wallichiana*) and Walnut (*Juglans regia*). The time desirable to achieve biosorption equilibrium is 80 min at temperatures in the range of 30 and 50 °C. The % removal of both As(III) and As(V) was, nonetheless, moderately unaffected by temperature, decreasing from 83.47826 at 30 °C to 66.08696 at 50 °C for As(III) and from 86.61538 at 30 °C to 69.74615 at 50 °C for As(V).

Biosorption activation energy

Biosorption rate constants k_{PSO} of both As(III) and As(V) were projected from experimental data at different temperatures assuming non-linear form of pseudo second-order kinetics. Parameters of Arrhenius equation were fitted using these rate constants for calculating temperature-independent rate parameters and biosorption type. A plot of ln k_{PSO} versus $1/T$ exhibited a straight line with slope $-E_a/R$ (Fig. S3; Table 8). The magnitudes of activation energy for As(III) and As(V) biosorption on TW/MnFe$_2$O$_4$ composite were 11.66 and 10.71 kJ/mol signifying that both the biosorption of As(III) and As(V) on the surface of TW/MnFe$_2$O$_4$ composite was activated chemisorption.

Characteristics of biosorbent

SEM–EDX analysis

The SEM images of acid-treated TW, the prepared unloaded TW/MnFe$_2$O$_4$ composite and TW/MnFe$_2$O$_4$ composite loaded with As(III) and TW/MnFe$_2$O$_4$ composite loaded with As(V) are shown in Fig. 13a–d, respectively. Figure 13a proves that many pores homogeneously pervaded on the pure acid-treated TW surface. It can be decided from Fig. 13b that manganese ferrite (MnFe$_2$O$_4$) particles with several diameters were randomly distributed on the acid-treated TW surface. Yet the surface of acid-treated TW was protected by several trivial aggregates of MnFe$_2$O$_4$ after

being merged; a slight porous structure could still be noticed, which conserved high biosorption capacities of the acid-treated TW. A modification in surface morphology from being smooth to rough and occupation of pores specified the As(III) and As(V) biosorption on the surface and pores of TW/MnFe$_2$O$_4$ composite giving it a rough texture (Agarwal et al. 2013).

The following EDX spectra of the unloaded and loaded composite were collected and shown in Fig. 13a–d. The attendances of iron, manganese and oxygen on the unloaded composite surface, and iron, manganese and oxygen, arsenic on the loaded composite surface were exposed clearly. This outcome again recognized the existence of MnFe$_2$O$_4$ particles on the acid-treated TW surface as well as biosorption of arsenic on the surface of composite.

FT-IR analysis

The biosorption capacity of heavy metal on many biosorbents is controlled by the existence of many active functional groups on the surface of biosorbent. The Fourier transform infrared spectra (FT-IR) study of unloaded as well as metal-loaded TW/MnFe$_2$O$_4$ composite at optimized batch experimental condition were examined for detecting the functional groups responsible mainly for the process of biosorption (Fig. 14). Table 9 indicates the wave number for the various functional groups existing in the unloaded TW/MnFe$_2$O$_4$ composite and As(III)- and As(V)-loaded biosorbent. Surface –OH and –NH groups were main active functional groups responsible for As(III) and As(V) biosorption as the wave number shifted from 3403.797 to 3419.225 cm^{-1} (As(III)) and to 3430.796 cm^{-1} (As(V)) (Singha and Das 2011). Some researchers have also stated that after the adsorption of

arsenic on the Fe–Ce and Fe–Mn adsorbents, the peak of hydroxyl groups reduced or vanished (Zhang et al. 2005, 2007). Aliphatic C–H stretching may be answerable for biosorption of As(III) and As(V) on TW/MnFe$_2$O$_4$ composite as wave number shifted from 2921.673 to 2930.233 and to 2923.602 cm^{-1}, respectively. Table 9 also shows the accountability of aliphatic acid C=O stretching for As(III) and As(V) biosorption by shifting the wave number from 1731.79 to 1729.862 and to 1728.992 cm^{-1}, respectively. Wave number shifted from 1639.223 to 1633.437 cm^{-1} (As(III)) and to 1633.437 cm^{-1} (As(V)) which provided the reactivity of unsaturated group like alkene for the biosorption process (Singha and Das 2011). Secondary amine groups may be answerable for biosorption of As(III) and As(V) on TW/MnFe$_2$O$_4$ composite since wave number shifted from 1542.798 to 1531.227 and to 1529.298 cm^{-1} as well as from 1525.441 to 1521.584 and to 1510.013 cm^{-1}, respectively (Malkoc and Nuhoglu 2006a; Uddin et al. 2009). Symmetric bending of CH$_3$ is also responsible which is concluded from the shift of the peak from 1448.301 cm^{-1} to 1444.444 cm^{-1} (As(III)) and to 1432.873 cm^{-1} (As(V)) (Malkoc and Nuhoglu 2006a). Wave number 1243.881 cm^{-1} shifted to 1237.209 and to 1241.952 cm^{-1} is assigned for –SO$_3$ stretching for the biosorption of As(III) and As(V), respectively. Wave number 1157.098 cm^{-1} shifted to 1159.027 cm^{-1} (As(III)) and to 1160.955 cm^{-1} (As(V)) indicated the C–O stretching of ether groups, active for the biosorption process (Malkoc and Nuhoglu 2006a, b).Wave number 1056.816 cm^{-1} shifted to 1052.959 cm^{-1} (As(III)) and to 1054.888 cm^{-1} (As(V)) indicated the Si–O stretching, active for the biosorption process (Lei et al. 2009). The band at 595.906 cm^{-1} could be recognized to the existence of Fe–O bond (McCafferty 2010; Ren et al. 2012),
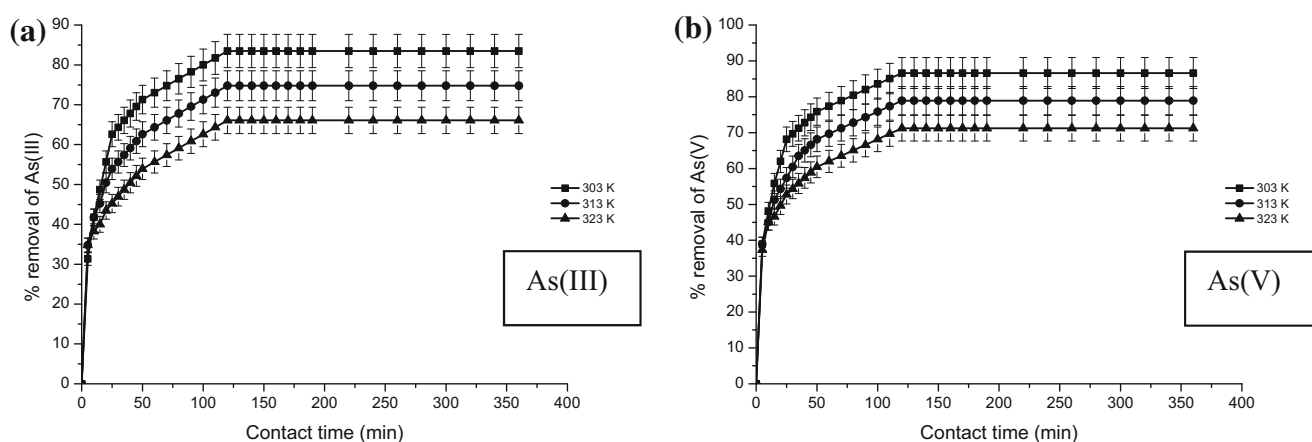

Fig. 12 Effect of temperature on contact time for **a** As(III) and **b** As(V) biosorption on the TW/MnFe$_2$O$_4$ composite [*T*: 30–50 °C; *t*: 0–360 min; *C*$_0$: 50 mg/L; pH: 7.0 (As(III)) and 4.0 (As(V)); *M*: 2 g/ L] (*error bars* represent means ± standard errors from the mean of duplicate experiments)

however, it shifted to 605.548 and 601.691 cm^{-1} after biosorption of As(III) and As(V), respectively. A distinctive peak at 558.76 cm^{-1} could be allotted for Mn–O bond (Kohler et al. 1997; Parida et al. 2004) and it had a different variability to 559.264 cm^{-1} for biosorption of both

Table 8 Activation energy for As(III) and As(V) biosorption onto TW/MnFe$_2$O$_4$ composite

Inorganic form	T (K)	k_{PSO} (g/mg min)	E_a (KJ/mol)
As(III)	303	0.00418	11.65654
	313	0.00513	
	323	0.00556	
As(V)	303	0.00531	10.70953
	313	0.00565	
	323	0.00692	

As(III) and As(V), respectively. The variation in wave number of Me–O bonds after biosorption of As(III) and As(V) exhibited that both Fe–O and Mn–O bonds were responsible for both MnFe$_2$O$_4$–As(III) and MnFe$_2$O$_4$–As(V) (Li et al. 2010; Ren et al. 2012). Existence of As(III) and As(V) on the biosorbent can be assured from the bands that appeared at 781.395 and 828.527 cm^{-1}, respectively (Mondal et al. 2007; Zhang et al. 2009; Aryal et al. 2010). It has to be cited here, that a perfect band was quite problematic to be acquired in the case of both As(III) and As(V) observed at 828.527 cm^{-1}. This may be due to various mechanisms involved in biosorption of As(III) and As(V). It should be well recognized that the As–O band after biosorption of arsenic was not visibly observed because of the broad overlapping peaks in this region (Li et al. 2010).
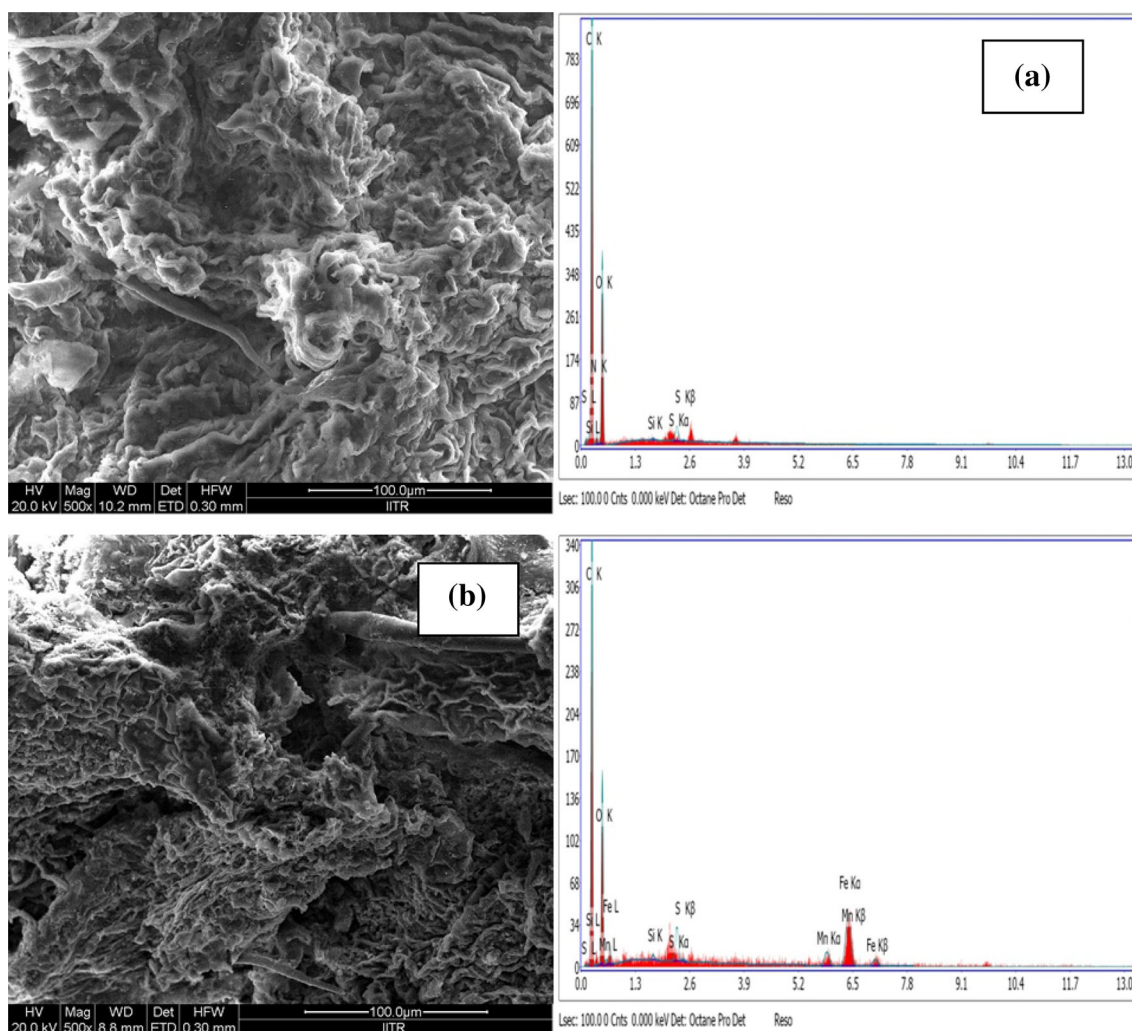

Fig. 13 Scanning electron micrographs (SEM) (500×) and EDX of **a** acid-treated TW, **b** TW/MnFe$_2$O$_4$ composite before biosorption, **c** TW/MnFe$_2$O$_4$ composite after biosorption of As(III) and **d** TW/MnFe$_2$O$_4$ composite after biosorption of As(V)

Fig. 13 continued

Fig. 14 FT-IR spectra of TW/MnFe$_2$O$_4$ composite (MTW) before biosorption, TW/MnFe$_2$O$_4$ composite after As(III) biosorption (MTW–As(III)) and TW/MnFe$_2$O$_4$ composite after As(V) biosorption (MTW–As(V))

Table 9 Wave number (cm^{-1}) for the dominant peak from FT–IR for As(III) and As(V) biosorption on $TW/MnFe_2O_4$ composite

Functional groups	TW/MnFe$_2$O$_4$ composite (MTW)	As(III)-loaded TW/MnFe$_2$O$_4$ composite (MTW–As(III))	As(V)-loaded TW/MnFe$_2$O$_4$ composite (MTW–As(V))
Surface O–H and N–H stretching	3403.797	3419.225	3430.796
Aliphatic C–H stretching	2921.673	2930.233	2923.602
Aliphatic acid C=O stretching	1731.79	1729.862	1728.992
Unsaturated group like alkene	1639.223	1633.437	1633.437
Secondary amine group	1542.798	1531.227	1529.298
Secondary amine group	1525.441	1521.584	1510.013
Symmetric bending of CH$_3$	1448.301	1444.444	1432.873
–SO$_3$ stretching	1243.881	1237.209	1241.952
C–O stretching of ether groups	1157.098	1159.027	1160.955
Si–O stretching	1056.816	1052.959	1054.888
Fe–O bond	595.906	605.548	601.691
Mn–O bond	558.76	559.264	559.264
As(III)–O	×	781.395	×
As(V)–O	×	×	828.527

Conclusions

- The present research exhibited that the $TW/MnFe_2O_4$ composite prepared via coprecipitation method, was applied successfully for the biosorption of both As(III) and As(V) from synthetically prepared wastewater.
- The optimum contact time and temperature for As(III) and As(V) biosorption were 110 min and 30 °C, respectively.
- Contact time essential for achievement of equilibrium improved with rising concentration, but, however, remained practically uninfluenced by rising temperature.
- The rate of biosorption of both As(III) and As(V) by $TW/MnFe_2O_4$ composite decreased with increasing concentration.
- By applying 14 different kinetic models and using the procedure of non-linear regression for curve fitting analysis (maximizing the correlation coefficient (R, R^2, $\overline{R^2}$) and minimizing the error values (SSE, reduced χ^2 and root-MSE) to evaluate optimum parameter sets, both the fractal-like exponential model as well as the Brouers–Weron–Sotolongo model were found suitable to predict the biosorption kinetic of As(III) on $TW/MnFe_2O_4$ composite according to GoFM values, and Brouers–Weron–Sotolongo kinetic model indicates that a complex mechanism of adsorption was seen suitable to forecast the biosorption kinetic of As(V) on $TW/MnFe_2O_4$ composite according to GoFM values.

- The results acquired from different mechanistic models indicated film diffusion as the governing factor over pore diffusion.
- The effective diffusivity estimated using Vermeulen's approximation indicated that the interactions between arsenic ions (either As(III) or As(V)) and GAC/$MnFe_2O_4$ composite were chemical in nature.
- The related thermodynamic parameters exposed that the biosorption of both As(III) and As(V) had been an exothermic process and spontaneous in nature.
- From Arrhenius equation, it was proved that the biosorption of As(III) and As(V) by $TW/MnFe_2O_4$ composite might be an ion exchange process.
- EDX analysis recognized the attendance of iron and manganese in the $TW/MnFe_2O_4$ composite and it also determined the fact that both As(III) and As(V) were adsorbed on the biosorbent.
- $TW/MnFe_2O_4$ composite can be used as a capable biosorbent for removal of both As(III) and As(V) from contaminated water sources.

link to the Creative Commons license, and indicate if changes were made.

References

Agarwal B, Balomajumder C, Thakur PK (2013) Simultaneous co-adsorptive removal of phenol and cyanide from binary solution using granular activated carbon. Chem Eng J 228:655–664

Al-Degs YS, El-Barghouthi MI, El-Sheikh AH, Walker GM (2008) Effect of solution pH, ionic strength, and temperature on adsorption behavior of reactive dyes on activated carbon. Dyes Pigments 77:16–23

Aryal M, Ziagova M, Liakopoulou-Kyriakides M (2010) Study on arsenic biosorption using Fe(III)-treated biomass of *Staphylococcus xylosus*. Chem Eng J 162:178–185

Atun G, Hisarli G (2003) Adsorption of carminic acid, a dye onto glass powder. Chem Eng J 95:241–249

Backes CA, McLaren RG, Rate AW, Swift RS (1995) Kinetics of cadmium and cobalt desorption from iron and manganese oxides. Soil Sci Soc Am J 59:778–785

Basha CA, Bhadrinarayana NS, Anantharaman N, Begum KMMS (2008) Heavy metal removal from copper smelting effluent using electrochemical cylindrical flow reactor. J Hazard Mater 152:71–78

Bianfang Z, Guide T, Zonglin Y, Zhenbiao W, Qingfen Y, Jianpo C (2007) Synthesis of magnetic manganese ferrite. J Wuhan Univ Technol Mater Sci Ed 22:514–517

Cheung CW, Porter JF, Mckay G (2001) Sorption kinetic analysis for the removal of cadmium ions from effluents using bone char. Water Res 35:605–612

Chiban M, Carja G, Lehutu G, Sinan F (2011) Equilibrium and thermodynamic studies for the removal of As(V) ions from aqueous solution using dried plants as adsorbents. Arab J Chem. doi:10.1016/j.arabjc.2011.10.002

Choong TSY, Chuah TG, Robiah Y, Koay FLG, Azni I (2007) Arsenic toxicity, health hazards and removal techniques from water: an overview. Desalination 217:139–166

Chubar N, Carvalho JR, Correia MJN (2004) Heavy metals biosorption on cork biomass: effect of the pretreatment. Colloids Surf A 238:51–58

Crini G, Badot PM (2008) Application of chitosan, a natural aminopolysaccharide, for dye removal from aqueous solutions by adsorption processes using batch studies: a review of recent literature. Prog Polym Sci 33:399–447

Dambies L (2004) Existing and prospective sorption technologies for the removal of arsenic in water. Sep Sci Technol 39:603–627

Edgar TF, Himmelblau DM (1989) Optimization of chemical processes. McGraw-Hill, New York

EPA (1998) Office of Ground water and drinking water, implementation guidance for the arsenic rule, EPA report-816-D-02-005, Cincinnati, USA

European commission Directive (1998) 98/83/EC, related with drinking water quality intended for human consumption. Belgium, Brussels

Ferguson JF, Gavis J (1972) A review of the arsenic cycle in nature waters. Water Res 6:1259–1274

Garelick H, Dybowska A, Valsami-Jones E, Priest ND (2005) Remediation technologies for arsenic contaminated drinking waters. J Soils Sedim 5:182–190

Gupta A, Chauhan VS, Sankararamakrishnan N (2009) Preparation and evaluation of iron–chitosan composites for removal of As(III) and As(V) from arsenic contaminated real life groundwater. Water Res 43:3862–3870

Hadi M, McKay G, Samarghandi MR, Maleki A, Aminabad MS (2012) Prediction of optimum adsorption isotherm: comparison of chi-square and log-likelihood statistics. Desalination Water Treat 49:81–94

Haerifar M, Azizian S (2012) Fractal-like adsorption kinetics at the solid/solution interface. J Phys Chem C 116:13111–13119

Haerifar M, Azizian S (2013) An exponential kinetic model for adsorption at solid/solution interface. Chem Eng J 215–216:65–71

Hanna OT, Sandall OC (1995) Computational methods in chemical engineering. Prentice-Hall International, New Jersey

Jeffers TH, Ferguson CR, Bennett PG (1991) Biosorption of metal contaminants using immobilized biomass—a laboratory study, report of investigations. Bureau of Mines, Salt Lake City

Kamsonlian S, Balomajumder C, Chand S (2012a) A potential of biosorbent derived from banana peel for removal of As(III) from contaminated water. IJCEA 3:269–275

Kamsonlian S, Suresh S, Majumder CB, Chand S (2012b) Biosorption of arsenic from contaminated water onto solid *Psidium guajava* leaf surface: equilibrium, kinetics, thermodynamics, and desorption study. Bioremed J 16:97–112

Kamsonlian S, Suresh S, Ramanaiah V, Majumder CB, Chand S, Kumar A (2012c) Biosorptive behaviour of mango leaf powder and rice husk for arsenic(III) from aqueous solutions. Int J Environ Sci Technol 9:565–578

Kavitha D, Namasivayam C (2007) Experimental and kinetic studies on methylene blue adsorption by coir pith carbon. Bioresour Technol 98:14–21

Khan AR, Al-Waheab IR, Al-Haddad A (1996) A generalized equation for adsorption isotherms for multi-component organic pollutants in dilute aqueous solution. Environ Technol 17:13–23

Kohler T, Armbruster T, Libowitzky E (1997) Hydrogen bonding and Jahn–Teller distortion in groutite, α–MnOOH, and Manganite, γ–MnOOH, and their relations to the manganese dioxides ramsdellite and their relations to the manganese dioxides ramsdellite and pyrolusite dioxides. J Solid State Chem 133:486–500

Korte NE, Fernando Q (1991) A review of arsenic (III) in ground water. Crit Rev Environ Control 21:1–39

Kundu S, Gupta AK (2006) Adsorptive removal of As(III) from aqueous solution using iron oxide coated cement (IOCC): evaluation of kinetic, equilibrium and thermodynamic models. Sep Purif Technol 51:165–172

Lei Y, Zheng-Fang Y, Mei-Ping T, Peng L, Jin-Ren N (2009) Removal of Cr^{3+} from aqueous solution by biosorption with aerobic granules. J Hazard Mater 165:250–255

Li Z, Deng S, Yu G, Huang J, Lima VC (2010) As(V) and As(III) removal from water by a Ce–Ti oxide adsorbent: behavior and mechanism. Chem Eng J 161:106–113

Liu X, Ao H, Xiong X, Xiao J, Liu J (2012) Arsenic removal from water by iron-modified bamboo charcoal. Water Air Soil Pollut 223:1033–1044

Lu S, Gibb SW (2008) Copper removal from wastewater using spent-grain as biosorbent. Bioresour Technol 99:1509–1517

Malkoc E, Nuhoglu Y (2006a) Removal of Ni(II) ions from aqueous solutions using waste of tea factory: adsorption on a fixed-bed column. J Hazard Mater B135:328–336

Malkoc E, Nuhoglu Y (2006b) Fixed bed studies for the sorption of chromium(VI) onto tea factory waste. Chem Eng Sci 61:4363–4372

McCafferty E (2010) Relationship between the isoelectric point (pHpzc) and the potential of zero charge (Epzc) for passive metals. Electrochimica Acta 55:1630–1637

McKay G, Otterburn MS, Sweeny AG (1981) Surface mass transfer process during colour removal from effluents using silica. Water Res 15:321–331

Meena AK, Mishra GK, Rai PK, Rajagopal C, Nagar PN (2005) Removal of heavy metal ions from aqueous solutions using carbon aerogel as an adsorbent. J Hazard Mater 122:161–170

Meng X, Bang S, Korfiatis GP (2000) Effects of silicate, sulfate, and carbonate on arsenic removal by ferric chloride. Water Res 34:1255–1261

Meng X, Korfiatis GP, Bang S, Bang KW (2002) Combined effects of anions on arsenic removal by iron hydroxides. Toxicol Lett 133:103–111

Michalak I, Chojnacka K, Witek-Krowiak A (2013) State of the art for the biosorption process—a review. Appl Biochem Biotechnol 170:1389–1416

Miretzky P, Munoz C, Carrillo-Chavez A (2008) Experimental binding of lead to a low cost on biosorbent: Nopal (*Opuntia streptacantha*). Bioresour Technol 99:1211–1217

Mohan D, Pittman CU Jr (2007) Arsenic removal from water/ wastewater using adsorbents—a critical review. J Hazard Mater 142:1–53

Mondal P, Majumder CB, Mohanty B (2006) Laboratory based approaches for arsenic remediation from contaminated water: recent developments. J Hazard Mater 137:464–479

Mondal P, Balomajumder C, Mohanty B (2007) A laboratory study for the treatment of arsenic, iron, and manganese bearing ground water using Fe^{3+} impregnated activated carbon: effects of shaking time, pH and temperature. J Hazard Mater 144:420–426

Mondal P, Majumder CB, Mohanty B (2009) Treatment of simulated arsenic contaminated groundwater using GAC-Cu in batch reactor: optimization of process parameters. Can J Chem Eng 87:766–778

Mostafapour FK, Bazrafshan E, Farzadkia M, Amini S (2013) Arsenic removal from aqueous solutions by *Salvadora persica* stem ash. J Chem 2013:1–8

Muroi M, Street R, McCormick PG (2001) Magnetic properties of ultrafine $MnFe_2O_4$ powders prepared by mechanochemical processing. Phys Rev B: Condens Matter 63:184414–184420

Naiya TK, Bhattacharya AK, Das SK (2009) Adsorption of Cd(II) and Pb(II) from aqueous solutions on activated alumina. J Colloid Interface Sci 333:14–26

Ncibi MC (2008) Applicability of some statistical tools to predict optimum adsorption isotherm after linear and non-linear regression analysis. J Hazard Mater 153:207–212

Ncibi MC, Ranguin R, Pintor MJ, Jeanne-Rose V, Sillanpää M, Gaspard S (2014) Preparation and characterization of chemically activated carbons derived from Mediterranean *Posidonia oceanica* (L.) fibres. J Anal Appl Pyrolysis 109:205–214

Neff JM (1997) Ecotoxicology of arsenic in the marine environment. Environ Toxicol Chem 16:917–927

Ngah WSW, Hanafiah MAKM (2008) Adsorption of copper on rubber (*Hevea brasiliensis*) leaf powder: kinetics, equilibrium and thermodynamic studies. Biochem Eng J 39:521–530

NHMRC, Australian Drinking Water Guidelines (1996) National Health and Medical Council, Agriculture and Resource Management Council of Australia and New Zealand, Commonwealth of Australia. PF S93

Nouri L, Ghodbane I, Hamdaoui O, Chiha M (2007) Batch sorption dynamics and equilibrium for the removal of cadmium ions from aqueous phase using wheat bran. J Hazard Mater 149:115–125

Parida KM, Mallick S, Mohapatra BK, Vibhuti N (2004) Misra, Studies on manganese–nodule leached residues: 1. Physicochemical characterization and its adsorption behavior toward Ni^{2+} in aqueous system. J Colloid Interface Sci 277:48–54

Park YJ, Ko JJ, Yun SL, Lee EY, Kim SJ, Kang-Lee BC (2008) Enhancement of bioremediation by *Ralstonia* sp. HM-1 in sediment polluted by Cd and Zn. Bioresour Technol 99:7458–7463

Parsons JG, Lopez ML, Peralta-Videa JR, Gardea-Torresdey JL (2009) Determination of arsenic(III) and arsenic(V) binding to microwave assisted hydrothermal synthetically prepared Fe_3O_4, Mn_3O_4, and $MnFe_2O_4$ nanoadsorbents. Microchem J 91:100–106

Pehlivan E, Tran TH, Ouédraogo WKI, Schmidt C, Zachmann D, Bahadir M (2013) Removal of As(V) from aqueous solutions by iron coated rice husk. Fuel Process Technol 106:511–517

Plazinski W, Rudzinski W, Plazinska A (2009) Theoretical models of sorption kinetics including a surface reaction mechanism: a review. Adv Colloid Interface Sci 152:2–13

Podder MS, Majumder CB (2015) SD/MnFe2O4 composite, a biosorbent for As (III) and As (V) removal from wastewater: optimization and isotherm study. J Mol Liq 212:382–404

Podder MS, Majumder CB (2016) Studies on the removal of As(III) and As(V) through their adsorption onto granular activated carbon/MnFe2O4 composite: isotherm studies and error analysis. Compos Interfaces 23(4):327–372

Qiu H, Lv L, Pan B-C, Zhang Q-J, Zhang W-M, Zhang Q-X (2009) Critical review in adsorption kinetic models. J Zhejiang Univ Sci A 10:716–724

Ramachandra TV, Ahalya N, Kanamadi R (2005) Biosorption: techniques and mechanisms. CES Technical Report 110. Centre for Ecological Sciences, Indian Institute of Science, Bangalore

Ranjan D, Talat M, Hasan SH (2009) Biosorption of arsenic from aqueous solution using agricultural residue 'rice polish'. J Hazard Mater 166:1050–1059

Ravenscroft P, Brammer H, Richards KS (2009) Arsenic pollution: a global synthesis. Wiley-Blackwell, UK

Ren Y, Li N, Feng J, Luan T, Wen Q, Li Z, Zhang M (2012) Adsorption of Pb(II) and Cu(II) from aqueous solution on magnetic porous ferrospinel MnFe2O4. J Colloid Interface Sci 367:415–421

Rengaraj S, Yeon J-W, Kim Y, Jung Y, Ha Y-K, Kim W-H (2007) Adsorption characteristics of Cu(II) onto ion exchange resins 252H and 1500H: kinetics, isotherms and error analysis. J Hazard Mater 143:469–477

Romero-Gonzalez J, Peralta-Videa JR, Rodrıguez E, Ramirez SL, Gardea-Torresdey JL (2005) Determination of thermodynamic parameters of Cr(VI) adsorption from aqueous solution onto *Agave lechuguilla* biomass. J Chem Thermodyn 37:343–347

Roy P, Mondal NK, Das K (2014) Modeling of the adsorptive removal of arsenic: a statistical approach. J Environ Chem Eng 2:585–597

Saqib ANS, Waseem A, Khan AF, Mahmood Q, Khan A, Habib A, Khan AR (2013) Arsenic bioremediation by low cost materials derived from Blue Pine (*Pinus wallichiana*) and Walnut (*Juglans regia*). Ecol Eng 51:88–94

Shao L, Ren Z, Zhang G, Chen L (2012) Facile synthesis, characterization of a MnFe2O4/activated carbon magnetic composite and its effectiveness in tetracycline removal. Mater Chem Phys 135:16–24

Sharma VK, Sohn M (2009) Aquatic arsenic: toxicity, speciation, transformations, and remediation. Environ Int 35:743–759

Singh TS, Pant KK (2006) Kinetics and mass transfer studies on the adsorption of arsenic onto activated alumina and iron oxide impregnated activated alumina. Water Qual Res J Can 41:147–156

Singha B, Das SK (2011) Biosorption of Cr(VI) ions from aqueous solutions: kinetics, equilibrium, thermodynamics and desorption studies. Colloids Surf B 84:221–232

Smedley PL, Kinniburgh DG (2002) A review of the source, behaviour and distribution of arsenic in natural waters. Appl Geochem 17:517–568

Tee TW, Khan ARM (1988) Removal of lead, cadmium and zinc by waste tea leaves. Environ Technol Lett 9:12–23

Tian Y, Wu M, Lin X, Huang P, Huang Y (2011) Synthesis of magnetic wheat straw for arsenic adsorption. J Hazard Mater 193:10–16

Uddin MT, Islam MA, Mahmud S, Rukanuzzaman M (2009) Adsorptive removal of methylene blue by tea waste. J Hazard Mater 164:53–60

Vaghetti JCP, Lima EC, Royer B, Cardoso NF, Martins B, Calvete T (2009) Pecan nutshell as biosorbent to remove toxic metals from aqueous solution. Sep Sci Technol 44:615–644

Vijayaraghavan K, Yun YS (2008) Bacterial biosorbents and biosorption. Biotechnol Adv 26:266–291

Volesky B (2001) Detoxification of metal-bearing effluents: biosorption for the next century. Hydrometallurgy 59:203–216

Wang JL, Chen JL (2006) Biosorption of heavy metals by *Saccharomyces cerevisiae*: a review. Biotechnol Adv 24:427–451

Wang S, Mulligan CN (2006) Natural attenuation processes for remediation of arsenic contaminated soils and groundwater. J Hazard Mater 138:459–470

Warrens MJ (2008) On similarity coefficients for 2×2 tables and correction for chance. Psychometrika 73:487–502

Weber WJ Jr, Morris JC (1963) Intraparticle diffusion during the sorption of surfactants onto activated carbon. J Sanit Eng Div Am Soc Civ Eng 89:53–61

WHO (1993) Guidelines for drinking water quality. World Health Organization, Geneva, p 41

Yadav KP, Tyagi BS (1987) Fly-ash for the treatment of Cd-rich effluent. Environ Technol Lett 8:225–234

Zakaria ZA, Zakaria Z, Surif S, Ahmad WA (2007) Biological detoxification of Cr(VI) using wood-husk immobilized *Acinetobacter haemolyticus*. J Hazard Mater 148:164–171

Zhang Y, Yang M, Dou XM, He H, Wang DS (2005) As(V) adsorption on an Fe–Ce bimetal oxide adsorbent: role of surface properties. Environ Sci Technol 39:7246–7253

Zhang GS, Qu JH, Liu HJ, Liu RP, Li GT (2007) Removal mechanism of As(III) by a novel Fe–Mn binary oxide adsorbent: oxidation and sorption. Environ Sci Technol 41:4613–4619

Zhang G, Liu H, Liu R, Qu J (2009) Adsorption behavior and mechanism of arsenate at Fe–Mn binary oxide/water interface. J Hazard Mater 168:820–825

Zhang S, Li X-Y, Chen JP (2010a) Preparation and evaluation of a magnetite-doped activated carbon fiber for enhanced arsenic removal. Carbon 48:60–67

Zhang S, Niu H, Cai Y, Zhao X, Shi Y (2010b) Arsenite and arsenate adsorption on coprecipitated bimetal oxide magnetic nanomaterials: $MnFe_2O_4$ and $CoFe_2O_4$. Chem Eng J 158:599–607

Zhang M, Gao B, Varnoosfaderani S, Hebard A, Yao Y, Inyang M (2013) Preparation and characterization of a novel magnetic biochar for arsenic removal. Bioresour Technol 130:457–462